

**INVESTIGATION OF ELECTRONIC, MECHANICAL AND
THERMOELECTRIC PROPERTIES OF QUATERNARY
HEUSLER COMPOUNDS ZrRhTiZ (Z= In, Al)**

A PROJECT REPORT

SUBMITTED IN PARTIAL FULFILMENT

OF THE REQUIREMENTS FOR THE AWARD OF THE

OF

DEGREE OF MASTER OF SCIENCE

PHYSICS

Submitted by:

Mohit Kumar (2K20/MSCPHY/15)

Vivek Kumar (2K20/MSCPHY/37)

Under the supervision of

Dr. Mukhtiyar Singh

Department of Applied Physics



DELHI TECHNOLOGICAL UNIVERSITY

(Formerly Delhi College of Engineering)

Bawana Road, New Delhi-11042

MAY, 2022

DECLARATION

We hereby certify that the work which is presented in the Major Project-II work entitled “Investigation of electronic, mechanical and thermoelectric properties of quaternary Heusler compounds $ZrRhTiZ$ ($Z = \text{In, Al}$)” in fulfillment of the requirement for the award of the Degree of Master of Science in Physics and submitted to the Department of **Applied physics**, Delhi Technological University, Delhi is an authentic record of our own, carried out during a period of June 2021 to May 2022, under the supervision of **Dr. Mukhtiyar Singh**.

The matter presented in this report has not been submitted by us for the award of any other Degree of this or any other Institute/University. The work has been published peer reviewed Scopus Indexed conference with the following details.

Title of the Paper: “Investigation of electronic, mechanical and thermoelectric properties of quaternary Heusler compounds $ZrRhTiZ$ ($Z = \text{In, Al}$)”

Author names: Vivek Kumar, Mohit Kumar and Mukhtiyar Singh.

Name of the conference: 13th International Conference on Materials Processing and Characterization.

Conference Date: April 22-24, 2022

Have you registered for the conference: Yes

Status of paper: Accepted

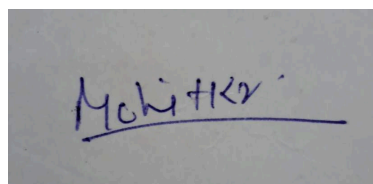
Date of Paper: 28th March 2022

Date of Acceptance: 7th April 2022

Date of Publication: 30th April 2022

Name (Roll no)

Vivek Kumar.

A rectangular box containing a handwritten signature in blue ink that reads "Mohit Kumar".

Vivek Kumar(2K20/MSCPHY/37), MohitKumar(2K20/MSCPHY/15)

SUPERVISOR CERTIFICATE

To the best of my knowledge, the above work has not been submitted in part or full for any Degree or Diploma to this University or Elsewhere. I further certify that the publication and indexing information given by the students is correct.

Place: Delhi

Date: 11th May 2022



(SUPERVISOR SIGN)

PLAGIARISM REPORT



Similarity Report ID: oid:27535:17104934

PAPER NAME

final plag report.pdf

WORD COUNT

5128 Words

CHARACTER COUNT

26942 Characters

PAGE COUNT

22 Pages

FILE SIZE

1.2MB

SUBMISSION DATE

May 11, 2022 2:31 PM GMT+5:30

REPORT DATE

May 11, 2022 2:33 PM GMT+5:30

● 9% Overall Similarity

The combined total of all matches, including overlapping sources, for each database.

- 4% Internet database
- 7% Publications database
- Crossref database
- Crossref Posted Content database
- 6% Submitted Works database

● Excluded from Similarity Report

- Bibliographic material
- Small Matches (Less than 10 words)
- Manually excluded sources
- Manually excluded text blocks

ACCEPTANCE RECORD



REGISTRATION RECORD



REGISTRATION FORM

PAPER ID: 422

Full Name: MOHIT KUMAR

Designation: Student (M.Sc - Physics)

Organization & Address: Delhi Technological University, Shahbad Daultpur, Main Bawana Road, Delhi-110042.

Mobile: +91-9910965358

Phone (o):

E-mail: mohitkumar_2k20mscphy15@dtu.ac.in

Amount paid: AMPT (Taylor and Francis) : Rs 15000 / USD 250

AIP conference proceedings : Rs 9000/ USD 175

Materials Today: Proceedings: 9000/ USD 175 ✓

Name of the Bank: HDFC BANK

Name of the account holder: Rohit Kumar

Date of the transaction: 10-April-2022

Online Transaction number: UPI Ref. - 210032287960

Registration Category: Educational Institution /Industry

Signature with Date

Mohit Kumar
10/04/2022

Correspondence Address:

ICMPC-2022

GOKARAJU RANGARAJU INSTITUTE OF ENGINEERING & TECHNOLOGY

BACHUPALLY, HYDERABAD-500090 TELANGANA, INDIA.

PHONE.NO: 091-9959870257

E-mail: icmpe-hyd@griet.ac.in

ACKNOWLEDGEMENT

We wish to express our profound gratitude and indebtedness to Dr. Mukhtiyar Singh, Associate Professor, Department of Applied Physics, Delhi Technological University for introducing the presented topic and for his inspiring guidance, constructive criticism, and valuable suggestion throughout the project work. Our thanks and appreciations go to everyone who has been involved directly or indirectly for their help, unwavering support, and valuable inputs in every part of this project. Lastly, our sincere thanks to all our friends and family who have patiently extended all sorts of help for accomplishing this task. In addition, we would like to thank Department of Applied Physics, Delhi Technological University for giving us the opportunity to work on this topic.

ABSTRACT

This work uses the first-principles method to investigate the electrical, mechanical, and transport properties of quaternary Heusler compounds ZrRhTiZ ($Z=\text{In, Al}$). ZrRhTiIn and ZrRhTiAl have lattice constants of 6.62 Å and 6.44 Å, respectively, which are in good agreement with previous studies. The alloys are semiconducting in the spin-down state, with indirect bandgaps of 0.39eV for ZrRhTiIn and 0.30eV for ZrRhTiAl , respectively, but metallic in the spin-up state, resulting in half-metallic ferromagnets. Several thermoelectric parameters are discussed in the paper, including the Seebeck coefficient, electrical and thermal conductivities, and power factor. For ZrRhTiAl and ZrRhTiIn alloys, the maximum reported power factors are $1.57 \times 10^{11} \text{Wm}^{-1}\text{K}^{-2}\text{s}^{-1}$ and $0.66 \times 10^{11} \text{Wm}^{-1}\text{K}^{-2}\text{s}^{-1}$, respectively. All of these features point to the possibility of using these materials in spintronic and thermoelectric devices.

CONTENTS

Cover Page	i
Declaration	ii
Supervisor certificate	iii
Plagiarism	iv
Acceptance	v
Registration	vi
Acknowledgement	vii
Abstract	viii
Contents	ix-x
List of Figures	xi-xii
List of Tables	xiii
List of Symbols, abbreviations	xiv

CHAPTER 1	INTRODUCTION	1
------------------	---------------------	----------

1.1.	Overview of the Thesis
------	------------------------

CHAPTER 2	COMPUTATION METHODOLOGY	2-3
------------------	--------------------------------	------------

- | | |
|-----|--|
| 2.1 | Wien2k |
| 2.2 | The Density Functional Theory (DFT) |
| 2.3 | LAPW Method |
| 2.4 | DFT & TB-mBJ Calculation of ZrRhTiZ (Z= In, Al) Alloys |

CHAPTER 3	RESULTS AND DISCUSSION	4-14
------------------	-------------------------------	-------------

- | | |
|-------|---------------------------------|
| 3.1 | Structural Properties |
| 3.2 | Electron Density |
| 3.3 | Electronic Properties |
| 3.4 | Transport Properties |
| 3.5.1 | Seebeck Coefficient |
| 3.5.2 | Electrical Conductivity |
| 3.5.3 | Electronic Thermal Conductivity |
| 3.5.4 | Power factor |

CHAPTER 4	CONCLUSION	15
REFERENES		16-21
RESEARCH PAPER		22-28
SCOPUS INDEXED		29

LIST OF FIGURES

Fig. 1(a). Crystal structure of ZrRhTiIn. Fig. 1(b). Crystal structure of ZrRhTiAl.

Fig. 2(a). Calculated Energy vs Volume curve of ZrRhTiIn.

Fig. 2(b). Calculated Energy vs Volume curve of ZrRhTiAl

Fig. 3(a). Electronic charge density contour in (110) plane for ZrRhTiIn

Fig. 3(b). Electronic charge density contour in (110) plane for ZrRhTiAl

Fig. 4(a). Spin polarized band structure of ZrRhTiIn within the TB-mBJ method for spin up state

Fig. 4(b). Spin polarized band structure of ZrRhTiIn within the TB-mBJ method for spin down state

Fig. 5(a). Spin polarized band structure of ZrRhTiAl within the TB-mBJ method for spin up state

Fig. 5(b). Spin polarized band structure of ZrRhTiAl within the TB-mBJ method for spin down state

Fig. 6(a). Variation of Seebeck Coefficient as a function of temperature for ZrRhTiAl

Fig. 6(b). Variation of Seebeck Coefficient as a function of temperature for ZrRhTiIn

Fig. 7(a). Variation of electrical conductivity as a function of temperature for ZrRhTiAl

Fig. 7(b). Variation of electrical conductivity as a function of temperature for ZrRhTiIn

Fig. 8(a). Variation of electrical conductivity as a function of temperature for ZrRhTiAl

Fig. 8(b). Variation of electrical conductivity as a function of temperature for ZrRhTiIn

Fig. 9(a). Variation of power factor as a function of temperature for ZrRhTiAl

Fig. 9(b). Variation of power factor as a function of temperature for ZrRhTiIn

LIST OF TABLES

TABLE No. 1. Calculated elastic parameters for the ZrRhTiIn and ZrRhTiAl

LIST OF SYMBOLS, ABBREVIATIONS

1. ZT - FIGURE OF MERIT
2. S - SEEBECK COEFFICIENT
3. T - ABSOLUTE TEMPERATURE
4. σ - ELECTRICAL CONDUCTIVITY
5. κ - THERMAL CONDUCTIVITY
6. κ_e - ELECTRICAL THERMAL CONDUCTIVITY
7. κ_l - LATTICE THERMAL CONDUCTIVITY
8. V - VOLTAGE
9. μ - MOBILITY

CHAPTER 1

INTRODUCTION

Heusler alloys (HA) -

Any of the first magnetic alloys, such as the Heusler alloy, consisting of metals that are not magnetic in their pure state. Fritz Heusler, a German mining engineer and chemist from the nineteenth century, was the inspiration for the alloys. Heusler alloys are made up of two parts copper, one part manganese, and one part tin, Aluminum, arsenic, antimony, bismuth, or boron can be used in place of tin, and silver can be used in place of copper. Other semiconducting materials, such as Half-Heusler (HH) alloys, have recently showed significant promise as thermoelectric materials. HH alloys are composed of low-cost, light-weight, and ecologically benign materials.

Due to their unusual structural, electrical, magnetic, mechanical, and thermodynamic properties, Heusler alloys (HA) have lately piqued scientific attention [1-9]. Due to its applications in spintronics [10], magnetoelectric [11], magnetocaloric [12], and ferromagnetic shape memory alloys [13], One of the most significant groups within the Heusler alloy family is equiatomic Quaternary Heusler alloy (EQH). Because of their low power dissipation. Because EQH alloys crystallize with the Y-structure, they are more suitable for a wide range of applications than other HA [14–16]. According to the stoichiometry, HA can be divided into three categories. (I) equiatomic Half-Heusler (XYZ), (ii) 2:1:1 full-Heusler (X₂YZ) [17-18], equiatomic quaternary Heusler (XX'YZ), in which X, X', and Y are transition metal elements, and Z is the main group element [19-21], ZrFeTiZ (Z= Si, Ge, Al), ZrFeTiZ (Z= In, Al, Ge), and ZrCoTiZ (Z= Al, Ga, Si, Ge) are three Zr-based EQH alloys that have been investigated for spin-gapless semiconductors [28-30].

The thermoelectric property of Heusler alloy allows it to transform heat energy into electrical energy (seebeck effects). It's a promising feature of HA since it can be used to convert heat to electricity in electronic refrigeration and power generation applications. The Seebeck coefficient, for example, can be used to determine thermoelectric efficiency (S), electrical conductivity (k), thermal conductivity (T), and the figure of merit (ZT) [31] as a function of the chemical potential. This work uses

DFT and the BoltzTraP code to report on the structural, electrical, mechanical, and thermoelectric properties ZrRhTiZ(Z=In, Al).

CHAPTER 2

COMPUTATIONAL METHODOLOGY

2.1. WIEN2k -

WIEN2k is a programme that allows you to calculate the electrical structure of solids using density functional theory (DFT). It employs one of the most precise methods for determining band structure: local orbitals(Lo) + full-potential (linearized) augmented plane-wave (LAPW) . WIEN2k is an all-electron system with several features and relativistic effects.

The Density functional theory (DFT) -

Neighborhood Spin Density Approximation (LSDA) is a useful and accurate approach in the DFT. A method for solving the crystals' multi-electron issue (the nucleus is in a certain position). Spin density (r) is a significant number utilized to compute general electricity.

$$E_{tot}(\rho_{\uparrow}, \rho_{\downarrow}) = T_s(\rho_{\uparrow}, \rho_{\downarrow}) + E_{ee}(\rho_{\uparrow}, \rho_{\downarrow}) + E_{Ne}(\rho_{\uparrow}, \rho_{\downarrow}) + E_{xc}(\rho_{\uparrow}, \rho_{\downarrow}) + E_{NN}$$

E_{NN} is considered disgusting. Motion electricity (of non-interacting particles), electron-electron repulsion, core electron attraction, exchange correlation energy, and so on were formerly classified as Coulomb electricity of a specific core and digital contribution. The LSDA is made up of approximations. E_{xc} expects that a collection of neighbor exchange correlated current densities μ_{xc} instances may be used to describe it. In general (spin up + spin down) and ii) the μ_{xc} shape chosen.

The LAPW method -

The linearized augmented plane wave (LAPW) method is one of the most accurate methods for detecting crystal electrical structure. It is based on density functional theory and addresses exchange and correlation using approaches such as the local spin density approximation (LSDA). In the literature, there are several types of LSDA potentials, although new advancements employing the generalized gradient approximation (GGA) are also available. On either a scalar or a vector relativistic method, relativistic effects in valence states can be incorporated. or a second variational technique that takes spin-orbit coupling into account The core states are treated in their entirety relativistically.

DFT & TB-mBJ Calculation of ZrRhTiZ (Z= In, Al) alloys -

The density functional theory was used to determine various parameters of the ZrRhTiZ (Z= In, Al) alloys. The exchange–correlation potentials were estimated using the Perdew–Burke–Ernzerhof generalized gradient approximation (GGA-PBE) and the integrated modified Becke– Johnson GGA (GGA + mBJ). The foundation set for this study was the linearized augmented plane wave with full potential formalism (FP LAPW) as implemented in the WIEN2k code. The Perdew–Burke–Ernzerhof generalized gradient approximation (GGA-PBE) and Tran–Blaha modified Becke–Johnson methods were used to derive the results (TB-mBJ).

The band gap results have been underestimated when using the GGA technique. To overcome erroneous estimated values, the Tran-Blaha modified Becke–Johnson approach was used. The structural relaxation for varying compositional occupancy was achieved by setting the plane wave cutoff (RKmax) to 7 and using a fine k-mesh with 8000 k-points in the Full Brillouin-zone to establish a converged ground state. Finer convergence has been achieved for energy and charge estimates at the cost of the convergence threshold 0.0001 Ry and 0.001 e, respectively. In addition, the separation of valence and core states has a cut-off energy of -6.0 Ry. The charge density Fourier expansion's highest vector magnitude (Gmax) = 13. The Boltzmann transport theory was used to determine the transport parameters of EQH ZrRhTiZ (Z= In, Al) (BoltzTraP code).

CHAPTER 3

RESULTS AND DISCUSSION

3.1 Structural Properties

According to reports, depending on the atom positions, the quaternary Heusler alloy $XX'YZ$ can take three different shapes. Type-1 includes X at 4c, X' at 4d, Y at 4b, and Z at 4a; Type-2 includes X at 4b, X' at 4d, Y at 4c, and Z at 4a; and Type-3 includes X at 4b, X' at 4d, Y at 4c, and Z at 4a. [25]. In Type-1, the current $ZrRhTiZ$ (In and Al) is shown to be the most stable [32-33]. Fig.1 (a) and (b) show the structure of $ZrRhTiIn$ and $ZrRhTiAl$ respectively. The energy minimization approach was used to get the equilibrium lattice parameter. To obtain the lattice parameter and energy for the ground state at equilibrium volume, the Birch-Murnaghan method is used. The obtained equilibrium lattice parameters for $ZrRhTiIn$ and $ZrRhTiAl$ are 6.63 Å and 6.45 Å , respectively. The volume versus energy curves of $ZrRhTiIn$ and $ZrRhTiAl$, (a) and (b), respectively, are depicted in Fig. 2.

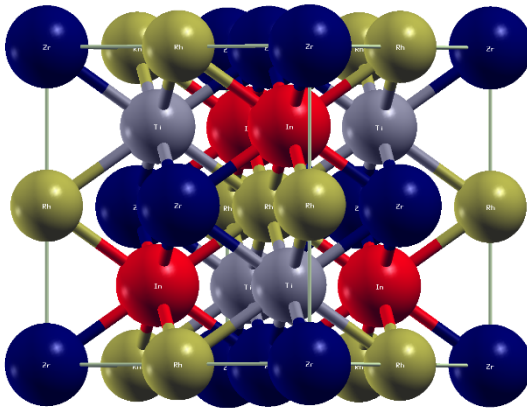


Fig. 1(a). Crystal structure of $ZrRhTiIn$.

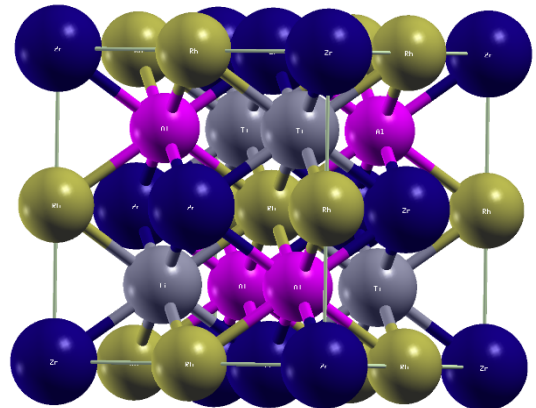


Fig. 1(b). Crystal structure of $ZrRhTiAl$.

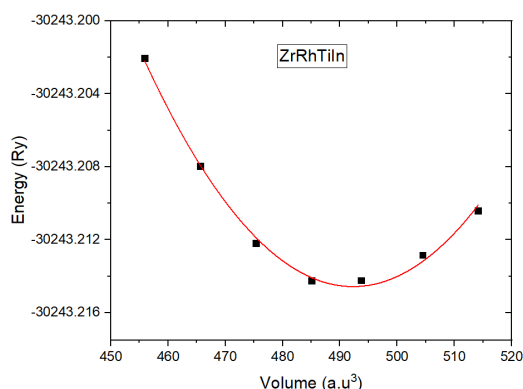


Fig. 2(a). Calculated Energy vs Volume curve of ZrRhTiIn.

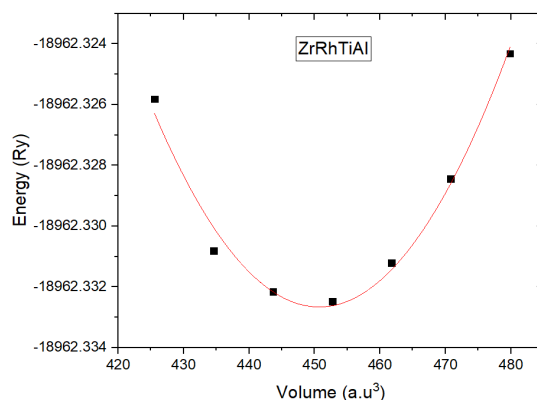


Fig. 2(b). Calculated Energy vs Volume curve of ZrRhTiAl

3.2 Electron Density

Electron density represents the probability of finding an electron at a specific location around an atom or molecule. In general, electrons are more likely to be discovered in areas where there is a large density of electrons. However, due to the uncertainty principle, it is impossible to pinpoint an electron's exact location at any one time. The density of electrons in a system containing a single electron is proportional to the square of the wavefunction. One technique for measuring electron density is X-ray diffraction crystallography.

When it comes to free radicals, the concept well known is spin density. This is the major dissimilarity among one spin's total electron density and the other spin's total electron density. The technique of neutron diffraction is used to map

Understanding the chemical characteristics of elements and atom bonding relies heavily on electron density maps. The electron density contour plot of both the EQH's along the 110 Plane is shown in Fig.3 (a) and (b), which helps us understand the chemical bonding in the alloys. Electron density graphs and contour maps can assist us comprehend d-d hybridization. The charge accumulations between Zr-Ti atoms are fewer than those between Rh-Ti atoms and Rh-Al/In atoms, showing that Zr-Ti interacts via ionic bond whereas Rh-Ti and Rh-Al/In interact by covalent band.

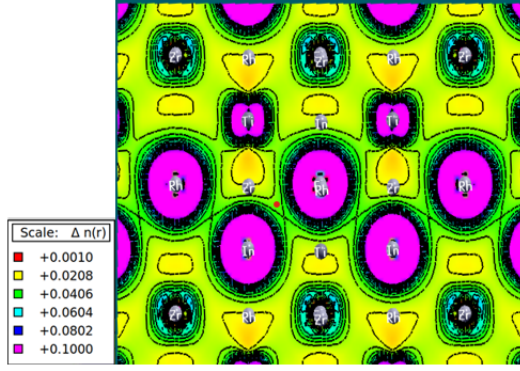


Fig. 3(a). ZrRhTiIn electronic charge density contour in (110) plane

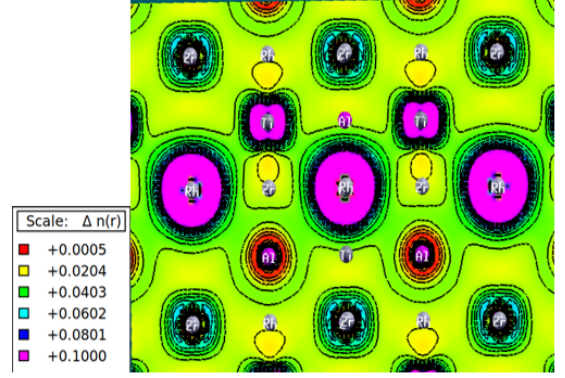


Fig. 3(b). ZrRhTiAl electronic charge density contour in (110) plane

3.3 Mechanical properties

Within the born-stability conditions, elastic parameters were estimated to predict the stability of the ZrRhTiZ (In, Al) alloy [34].

$$C_{11} - C_{12} > 0, C_{11} + 2C_{12} > 0, C_{44} > 0$$

The elastic parameters are shown in Table 1. Each material is found to satisfy the stability requirements and thus be mechanically stable.

The following formula is used to compute the bulk modulus B:

$$B = \frac{C_{11} + C_{12}}{3} \quad (1)$$

shear modulus G , compressibility and Young's modulus E, , and are determined using the elastic parameters [35].

$$E = \frac{9BG_H}{3B + G_H} \quad (2)$$

$$G = C_{44} \quad (3)$$

$$\beta = \frac{1}{B} \quad (4)$$

The Poisson coefficient (σ) is a measurement of a material's ductility or fragility, and it's written like this:

$$\sigma = \frac{1}{2} - \frac{E}{6B} \quad (5)$$

Furthermore, the Zener's value (A) can be calculated using the following equation:

$$A = \frac{2C_{44}}{C_{11} - C_{12}} \quad (6)$$

If A equals one unit, the crystal is said to be isotropic; otherwise, the crystal is said to be anisotropic.

The same formula applies to Reuss shear modulus, Cauchy's pressure, Voigt shear modulus and Hill shear modulus.

$$G_p = C_{12} - C_{44} \quad (7)$$

$$G_R = \frac{5(C_{11}+C_{12})C_{44}}{4C_{44}+3(C_{11}-C_{12})} \quad (8)$$

$$G_v = \frac{C_{11}-C_{12}+3C_{44}}{5} \quad (9)$$

$$G_H = \frac{G_R+G_v}{2} \quad (10)$$

$$Pugh's\ ratio = \frac{B}{G} \quad (11)$$

TABLE NO. 2. Elastic parameters of ZrRhTiIn and ZrRhTiAl

Elastic parameters	ZrRhTiIn	ZrRhTiAl
C_{11} (GPa)	144.381	134.209
C_{12} (GPa)	118.126	128.502
C_{44} (GPa)	44.592	54.788
$C_{11} - C_{12}$ (GPa)	27.552	12.737
$C_{11} + 2C_{12}$ (GPa)	380.663	391.213
G (shear modulus) (GPa)	44.592	54.788
Cp (Cauchy's pressure) (GPa)	73.534	73.714
B (Bulk modulus) (GPa)	126.445	126.395
β (compressibility)	0.0079	0.0079
Pugh's ratio (B/G)	2.835	2.306
A (Zener's value)	3.2369	8.602
V (Poisson coefficient)	0.207	0.41146

The Pugh's ratio (B/G) can be used to determine if a material is ductile (>1.75) or

brittle (1.75). The computed Pugh's ratio for ZrRhTiIn is 2.83, indicating that the material is ductile, whereas the Pugh's ratio for ZrRhTiAl is 2.30, indicating that the material is also ductile. The Cauchy pressure ($C_{12} - C_{44}$), which is positive for ductile materials and negative for brittle, supports this. For non-central force $\nu > 0.25$ and $0.25 < \nu < 0.50$ for central force, the Poisson ratio forecasts the nature of the forces present. The computed Poisson ratio for ZrRhTiIn is 0.20, indicating that there is a non-central force present, whereas it is 0.41 for ZrRhTiAl, indicating that there is a central force present. The Poisson ratio can also aid in better understanding the nature of bonding. If it is close to or greater than 0.25, it indicates ionic bonding, whereas less than 0.25 indicates covalent bonding. The Zener's value (A) for ZrRhTiIn is 3.23 and for ZrRhTiAl is 8.60, indicating that both materials are anisotropic (other than unity).

3.3 Electronic Properties

The TB-mBJ potential was used to calculate The Brillouin zone's spin-polarized band structure with high symmetry orientations. Both ZrRhTiZ (Z= In, Al) materials a metallic character when spin up and a semiconductor character when spin down, with a band gap approaching Fermi. ZrRhTiIn has a band gap of 0.38 eV, while ZrRhTiAl has a band gap of 0.29 eV. The maximal valence band and the minimum conduction band of the ZrRhTiZ (Z=In, Al) alloys are situated at Γ and L, respectively, indicating an indirect band (Fig. 4 and 5). The occurrence of a band gap at the fermi level in the down spin state implies that these alloys have 100 percent spin polarization.

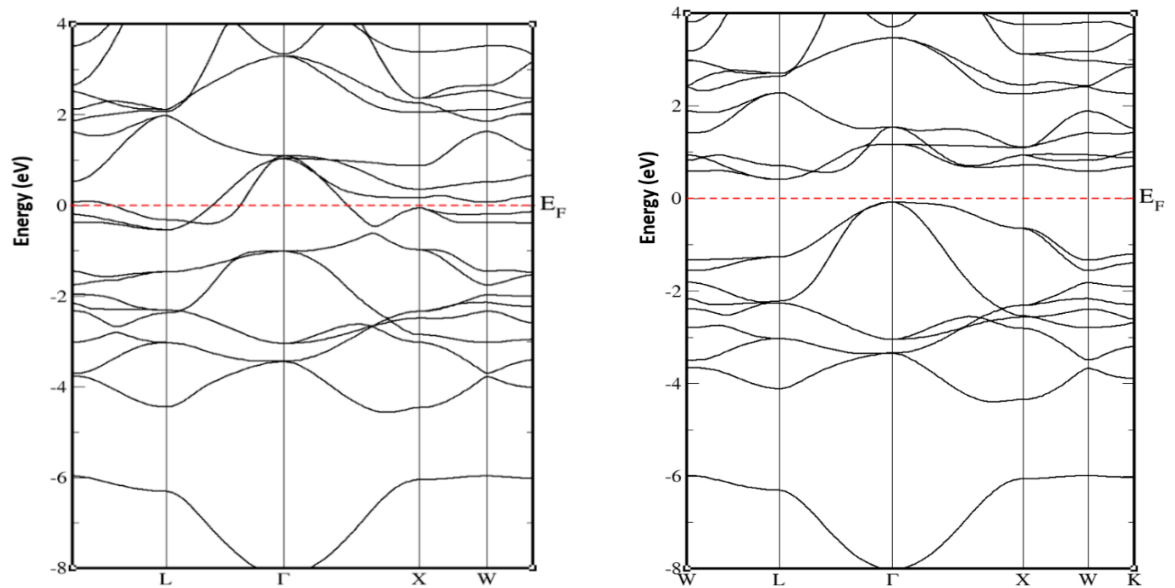


Fig. 4(a). Within the TB-mBJ approach for spin up state, spin polarised band structure of ZrRhTiIn.

Fig. 4(b). Within the TB-mBJ approach for spin down state, spin polarised band structure of ZrRhTiIn.

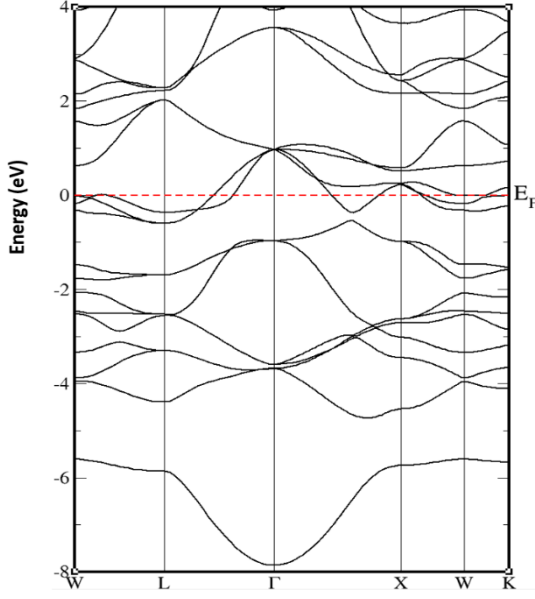


Fig. 5(a). Within the TB-mBJ approach for spin up state, spin polarised band structure of ZrRhTiAl

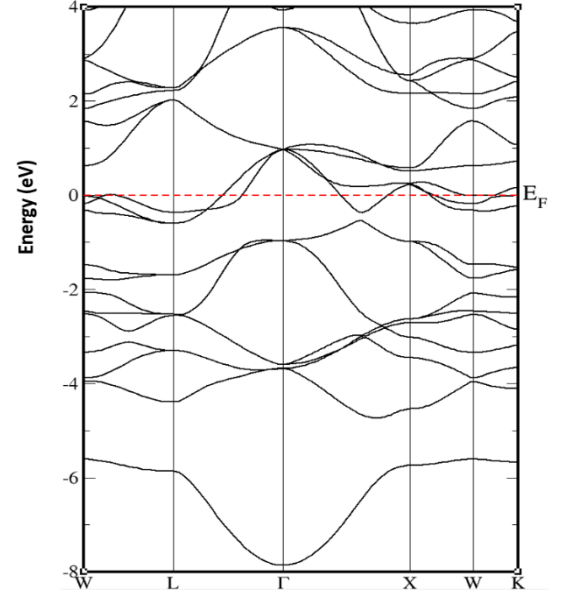


Fig. 5(b). Within the TB-mBJ approach for spin down state, spin polarised band structure of ZrRhTiAl

There are three possible explanations for the origin of the band gap in Heusler alloy. Covalent bonding, d-d hybridization, and charge transfer are the three processes. The hybridization of the Zr-4d and Rh-4d atoms in the compounds produces 5 bonding bands (BB) and 5 non-bonding (NB) bands, with $3t_{2g}$ and $2e_g$ in BB and $2e_u$ and $3t_u$ in NB. The bonding and antibonding bands were formed by the Ti 3d orbital hybridizing with the 4d orbitals of 5 Zr-Rh BB, while the 5 NB 4d orbitals remained unhybridized. As a result, 15d orbitals are assigned to the spin-up and spin-down states, which are labelled $3t_{2g}$, $2e_g$, $2e_u$, $3t_{1u}$, $3t_{2g}$, $2e_g$, $3t_{2g}$, $2e_g$, $3t_{1u}$, $3t_{2g}$, $2e_g$, $3t_{2g}$, Z (In, Al) has totally filled 1s and 3p orbitals

3.4 Transport property

Thermal conductivity (κ), Seebeck coefficient (S), , Electrical conductivity (σ), and power factor (PF) as a function of temperature up to 1200 K were investigated using the semiclassical Boltzmann transport theory-based BoltzTraP code [36]. The following equations are used to compute the electrical conductivity and Seebeck coefficient using the general Boltzmann transport equation [37]:

$$\sigma_{\alpha\beta}(\epsilon) = \sum_i \tau v_{\alpha}(i, k) v_{\beta}(i, k) \frac{\delta(\epsilon - \epsilon_{i,k})}{\delta\epsilon} \quad (12)$$

$$S = \frac{E_i}{T} \Delta j T^{-1} = (\sigma)^{-1} v_{\alpha j} \quad (13)$$

Where, ϵ , N and τ are band energy, number of k-points and relaxation time, respectively. $v_{\alpha}(i, k)$ is group velocity & The tensor indices of electrical conductivity are α and β [37].

3.4.1 Seebeck Coefficient

Thomas Johann Seebeck, a German physicist, discovered in 1821 that when two strips of different electrically conducting materials were separated along their length but not across their width, united at their ends by two "legs," a magnetic field formed around the legs as long as the two junctions had a temperature difference. After his observations, which he presented the next year, the Seebeck effect was named. Seebeck, on the other hand, could not determine the source of the magnetic field. The magnetic fields produced by the two metal-strip legs are equal but opposite. An electric potential differential across the junctions causes these currents, which is caused by temperature fluctuations in the materials. If one link is open, no current exists, but the temperature differential stays constant.

A material's Seebeck coefficient, commonly known as thermopower or thermoelectric power, magnitude of an induced thermoelectric voltage in response to a temperature gradient across a material is measured, it is brought about by the Seebeck effect (one of the thermoelectric effects). In some materials, the Seebeck coefficient can be negative for negatively charged carriers (electrons) and positive for positively charged

carriers (electrons) (electron holes). Over a wide temperature range, the Linseis LSR provides for simultaneous measurement of the Seebeck coefficient and four terminal electrical resistivity of a bulk or thin film sample.

The Seebeck Coefficient describes the amount of an induced thermoelectric voltage caused by a temperature differential across a material [38]. Thermoelectric applications benefit from materials with a high Seebeck Coefficient [39]. The Seebeck Coefficient in relation to temperature for contemporary alloys is shown in Figure 6 (a-b). The Seebeck Coefficient found for the ZrRhTiAl is positive for the majority of the temperature range, indicating that the alloy is a P-type semiconductor, as shown in Fig.6 (a). The importance of Seebeck At 150K, the coefficient starts at 15.7 VK^{-1} , drops to -1.83 VK^{-1} at 550K, and then rises to 4.01 VK^{-1} at 1200K. Its value at 300K is 2.67 VK^{-1} , which is not very high when compared to other materials.

The fluctuation of the Seebeck coefficient for ZrRhTiIn alloys is shown in Fig.6 (b), and It's worth noting that it is negative for most temperature ranges, indicating that this alloy is an N-type semiconductor. Its value begins at -101.2 VK^{-1} at 150 K, drops to -9.20 VK^{-1} at 350 K, and then returns to a positive value with a rise in temperature up to 800 K, with a value of 5.47 VK^{-1} . Its value at room temperature is roughly -25.40 VK^{-1} , indicating that it is more energy efficient than the former.

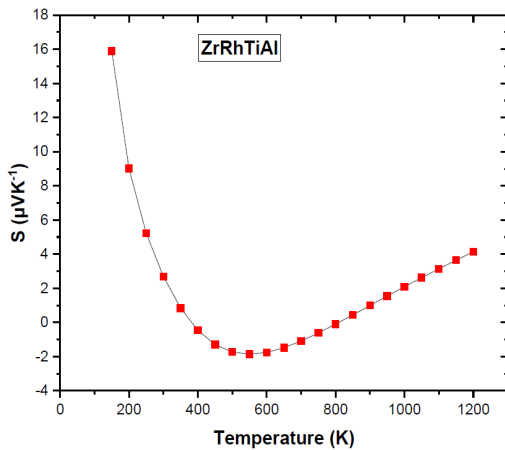


Fig. 6(a). Temperature-dependent variation of the Seebeck Coefficient for ZrRhTiAl

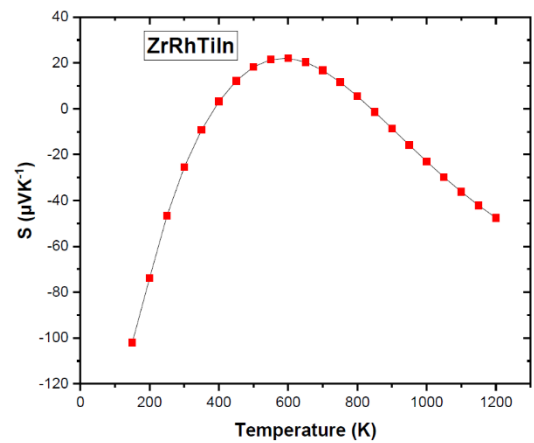


Fig. 6(b). Temperature-dependent variation of the Seebeck Coefficient for ZrRhTiIn

3.4.2 Electrical conductivity (σ/τ)

Electrical conductivity [40] measures the amount of electric charge or heat that can travel across the Fermi level. Figure 7 depicts the fluctuation of electrical conductivity(σ) with temperature(T) for both alloys (a-b). The electrical conductivity value increases with temperature from $65.6 \times 10^{20} (\Omega\text{ms})^{-1}$ at 150K to $73.0 \times 10^{20} (\Omega\text{ms})^{-1}$ at 600K and then starts to drop until $71.7 \times 10^{20} (\Omega\text{ms})^{-1}$ at 1200K. The electrical conductivity value at room temperature is $71.23 \times 10^{20} (\Omega\text{ms})^{-1}$ for ZrRhTiAl alloy. The electrical conductivity of the ZrRhTiIn alloy shows a roughly linear fluctuation with temperature, as shown in fig.7 (b). Electrical conductivity increases with increasing temperature, starting at $0.049 \times 10^{20} (\Omega\text{ms})^{-1}$ at 150K. At 1200K, the value of σ/τ is $0.535 \times 10^{20} (\Omega\text{ms})^{-1}$, while the value of electrical conductivity at ambient temperature is $\sim 0.103 \times 10^{20} (\Omega\text{ms})^{-1}$.

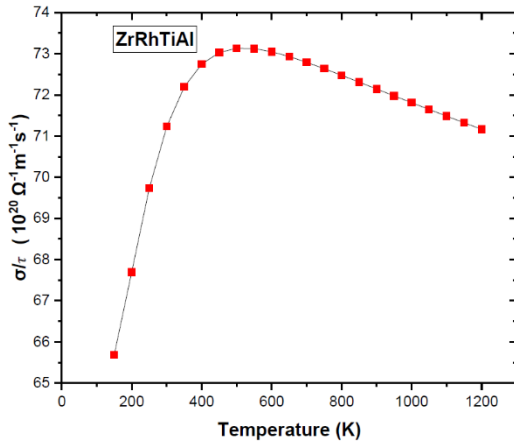


Fig. 7(a). Variation of electrical conductivity as a function of temperature for ZrRhTiAl

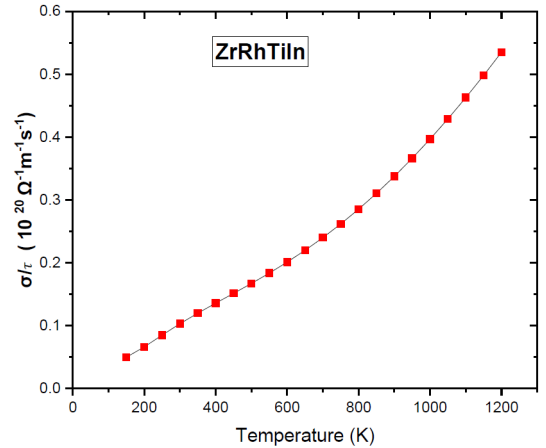


Fig. 7(b). Variation of electrical conductivity as a function of temperature for ZrRhTiIn

3.4.3 Electronic Thermal conductivity (κ_e/τ)

Since a material's thermal conductivity is inversely proportional to its thermoelectric performance, it should be kept as low as possible in order to achieve a better merit score. [41]. The electrical component of thermal conductivity varies as a function of temperature, as seen in Fig.8(a-b). The electronic thermal conductivity of the ZrRhTiAl increases linearly from $2.72 \times 10^{16} \text{ (W m}^{-1}\text{K}^{-1}\text{s}^{-1}\text{)}$ to $19.4 \times 10^{16} \text{ (Wm}^{-1}\text{K}^{-1}\text{s}^{-1}\text{)}$, as shown in Figure 12(a). At room temperature, electronic thermal conductivity equals $5.64 \times 10^{16} \text{ (Wm}^{-1}\text{K}^{-1}\text{s}^{-1}\text{)}$. Similarly, Fig.7(b) depicts that, with increasing temperature, the electrical thermal conductivity of ZrRhTiIn grows exponentially from $0.043 \times 10^{16} \text{ (Wm}^{-1}\text{K}^{-1}\text{s}^{-1}\text{)}$ to $0.568 \times 10^{16} \text{ (Wm}^{-1}\text{K}^{-1}\text{s}^{-1}\text{)}$, with a room temperature value of $\sim 0.017 \times 10^{16} \text{ (W m}^{-1}\text{K}^{-1}\text{s}^{-1}\text{)}$. Because ZrRhTiIn has a lower value than ZrRhTiAl, the former will be more beneficial because heat dissipation in the ZrRhTiIn alloy is lower.

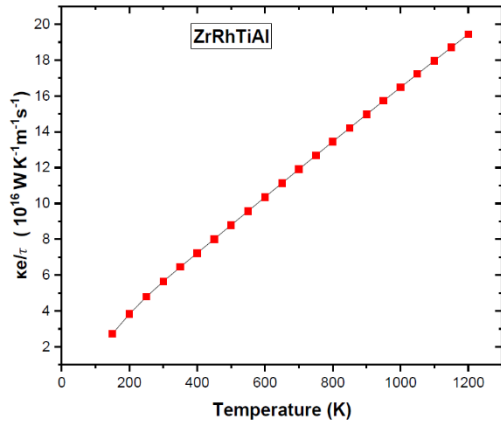


Fig. 12(a). Variation of electrical conductivity for ZrRhTiAl as a function of temperature

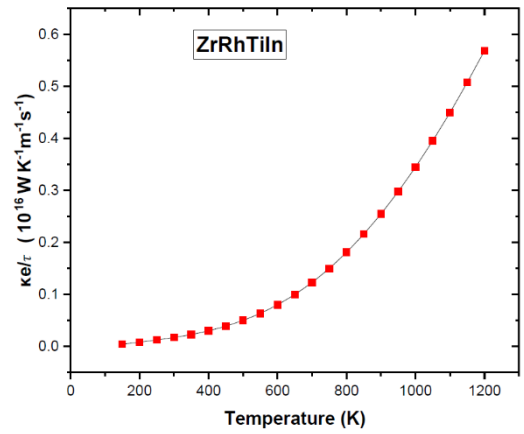


Fig. 12(b). Variation of electrical conductivity for ZrRhTiIn as a function of temperature

3.4.4 Power Factor

The power factor is a parameter which determines the efficiency of the material for the thermoelectric application. The power factor is defined by,

$$PF = \frac{S^2 \sigma}{\tau} \quad (15)$$

σ/τ is the electrical conductivity, and S is the Seebeck coefficient [42]. Figure 8(a-b) shows the PF versus temperature for both EQHs. Fig.13(a) shows the plot of PF against temperature for ZrRhTiAl from 150K to 1200K. It can be shown that the PF reaches its maximum value of $\sim 17.74 \times 10^{11} \text{ W m}^{-1} \text{ K}^{-2} \text{ s}^{-1}$ at 150K, then declines till it reaches $\sim 0.2101 \times 10^{11} \text{ W m}^{-1} \text{ K}^{-2} \text{ s}^{-1}$ at 500K, then grows slowly or becomes almost constant. At room temperature, the value of PF for ZrRhTiAl alloy is $\sim 1.57 \times 10^{11} \text{ W m}^{-1} \text{ K}^{-2} \text{ s}^{-1}$. Similarly, for the ZrRhTiIn alloy, Fig.13. (b) shows the fluctuation of PF as a function of temperature. The PF value at 150K is $5.56 \times 10^{11} \text{ W m}^{-1} \text{ K}^{-2} \text{ s}^{-1}$, while the PF value at 1200K is $\sim 12.11 \times 10^{11} \text{ W m}^{-1} \text{ K}^{-2} \text{ s}^{-1}$. At room temperature, the value of PF is found to be $\sim 0.66 \times 10^{11} \text{ W m}^{-1} \text{ K}^{-2} \text{ s}^{-1}$.

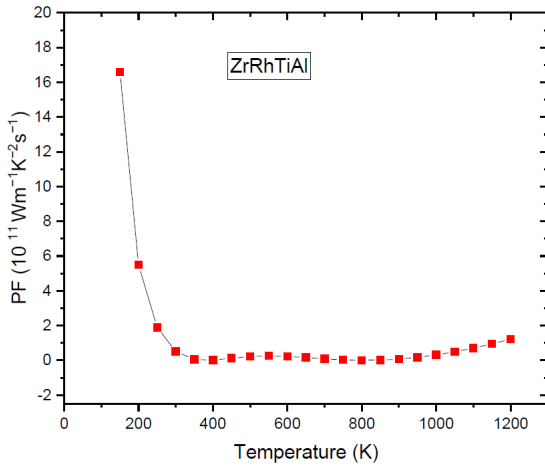


Fig.8(a). Variation of ZrRhTiAl's power factor as a function of temperature

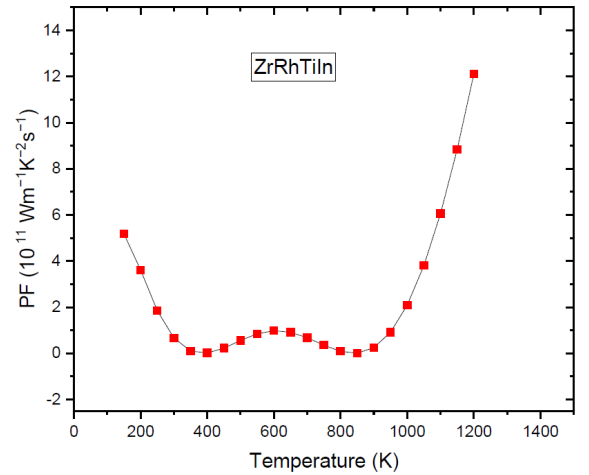


Fig. 8(b). Variation of ZrRhTiIn's power factor as a function of temperature

CHAPTER 4

Conclusions

We investigated the electrical, mechanical, and thermoelectric properties of the equiatomic quaternary Heusler alloys ZrRhTiIn and ZrRhTiAl using a density functional theory approach and semi-classical methods in this study. Both alloys were discovered to be semiconducting with an indirect band gap in the spin-down state. They are suitable for thermoelectric applications due to their tiny band gap. The obtained band gap results are consistent with those previously reported[25]. At 300K, the Seebeck coefficient for ZrRhTiIn is $-25.40 \mu\text{VK}^{-1}$ and for ZrRhTiAl is $\sim 2.67 \mu\text{VK}^{-1}$, with Power factors of $\sim 1.57 \times 10^{11} \text{ W m}^{-1}\text{K}^{-2}\text{s}^{-1}$ and $\sim 0.66 \times 10^{11} \text{ W m}^{-1}\text{K}^{-2}\text{s}^{-1}$ respectively. In comparison to ZrRhTiAl, ZrRhTiIn is a more promising thermoelectric material. Although the reported values are insufficient for use, they can be enhanced by using appropriate electron and hole doping.

References -

[1]	J. Winterlik, G. H. Fecher, A. Thomas, and C. Felser, "Superconductivity in palladium-based Heusler compounds," <i>Physical Review B - Condensed Matter and Materials Physics</i> , vol. 79, no. 6, Feb. 2009, doi: 10.1103/PhysRevB.79.064508.
[2]	I. Galanakis, P. H. Dederichs, and N. Papanikolaou, "Slater-Pauling behavior and origin of the half-metallicity of the full-Heusler alloys," <i>Physical Review B - Condensed Matter and Materials Physics</i> , vol. 66, no. 17, pp. 1–9, 2002, doi: 10.1103/PhysRevB.66.174429.
[3]	R. Panguluri, G. Tsoi, B. Nadgorny, S. H. Chun, N. Samarth, and I. I. Mazin, "Point Contact Spin Spectroscopy of Ferromagnetic MnAs Epitaxial Films."
[4]	SrishtiSingh,Dinesh C.Gupta.Lanthanum based quaternary Heusler alloys LaCoCrX (X = Al, Ga): Hunt for half-metallicity and high thermoelectric efficiency.Results in Physics, Volume 13, June 2019, 102300.
[5]	Alqurashi, H., Hamad, B. Magnetic structure, mechanical stability and thermoelectric properties of VTiRhZ (Z = Si, Ge, Sn) quaternary Heusler alloys: first-principles calculations. <i>Appl. Phys. A</i> 127, 799 (2021).
[6]	Ab Quayoom Seh, Dinesh C. Gupta. Quaternary Heusler alloys a future perspective for revolutionizing conventional semiconductor technology.Journal of Alloys and Compounds,Volume 871, 5 August 2021, 159560.
[7]	Haleoot, Raad & Hamad, Bothina. (2019). Thermodynamic and thermoelectric properties of CoFeYGe (Y= Ti, Cr) quaternary Heusler alloys: First principle calculations. <i>Journal of Physics: Condensed Matter</i> . 32. 10.1088/1361-648X/ab5321.
[8]	A, Afaq & Asif, Ayesha & Bakar, Abu & Khan, Muhammad & Munir, H. & B, Shanian & Asif, M.. (2019). DFT study of CuCoMnX (X = Si, Sn, Sb) quaternary Heusler alloys for phonon spectra. <i>Modern Physics Letters B</i> . 33. 10.1142/S0217984919501550.

[9]	S. Berri, “Computational Study of Structural, Electronic, Elastic, Half-Metallic and Thermoelectric Properties of CoCrScZ (Z=Al, Si, Ge, and Ga) Quaternary Heusler Alloys”, doi: 10.1007/s10948-020-05638-4/Published.
[10]	S. Berri, “First-principles Study on Half-metallic Properties of the CoMnCrSb Quaternary Heusler Compound,” <i>Journal of Superconductivity and Novel Magnetism</i> , vol. 29, no. 5, pp. 1309–1315, May 2016, doi: 10.1007/s10948-016-3404-7.
[11]	K. Özdoğan, E. Şaşıoğlu, and I. Galanakis, “Slater-Pauling behavior in LiMgPdSn-type multifunctional quaternary Heusler materials: Half-metallicity, spin-gapless and magnetic semiconductors,” <i>Journal of Applied Physics</i> , vol. 113, no. 19, May 2013, doi: 10.1063/1.4805063.
[12]	A. Planes, L. Māosa, and M. Acet, “Magnetocaloric effect and its relation to shape-memory properties in ferromagnetic Heusler alloys,” <i>Journal of Physics Condensed Matter</i> , vol. 21, no. 23, 2009, doi: 10.1088/0953-8984/21/23/233201.
[13]	L. Bainsla and K. G. Suresh, “Equiatomic quaternary Heusler alloys: A material perspective for spintronic applications,” <i>Applied Physics Reviews</i> , vol. 3, no. 3. American Institute of Physics Inc., Sep. 01, 2016. doi: 10.1063/1.4959093.
[14]	K. Inomata <i>et al.</i> , “Highly spin-polarized materials and devices for spintronics,” in <i>Science and Technology of Advanced Materials</i> , Mar. 2008, vol. 9, no. 1. doi: 10.1088/1468-6996/9/1/014101.
[15]	C. Felser, G. H. Fecher, and B. Balke, “Spintronics: A challenge for materials science and solid-state chemistry,” <i>Angewandte Chemie - International Edition</i> , vol. 46, no. 5. pp. 668–699, 2007. doi: 10.1002/anie.200601815.
[16]	R. Benabboun, D. Mesri, A. Tadjer, A. Lakdja, and O. Benhelal, “Half-Metallicity Ferromagnetism in Half-Heusler XCaZ (X = Li, Na; Z = B, C) compounds: an Ab Initio Calculation,” <i>Journal of Superconductivity and Novel Magnetism</i> , vol. 28, no. 9, pp. 2881–2890, Sep. 2015, doi:

	10.1007/s10948-015-3113-7.
[17]	R. Ahmad and N. Mehmood, “A First Principle Study of Half-Heusler Compounds CrTiZ (Z = P, As),” <i>Journal of Superconductivity and Novel Magnetism</i> , vol. 31, no. 1, pp. 257–264, Jan. 2018, doi: 10.1007/s10948-017-4209-z.
[18]	G. Y. Gao, L. Hu, K. L. Yao, B. Luo, and N. Liu, “Large half-metallic gaps in the quaternary Heusler alloys CoFeCrZ (Z = Al, Si, Ga, Ge): A first-principles study,” <i>Journal of Alloys and Compounds</i> , vol. 551, pp. 539–543, Feb. 2013, doi: 10.1016/j.jallcom.2012.11.077.
[19]	R. Paudel and J. Zhu, “Structural, electronic, magnetic, elastic, and thermal properties of Co-based equiatomic quaternary Heusler alloys,” <i>Journal of Magnetism and Magnetic Materials</i> , vol. 453, pp. 10–16, May 2018, doi: 10.1016/j.jmmm.2017.12.103.
[20]	G. D. Liu <i>et al.</i> , “Physical and electronic structure and magnetism of Mn ₂ NiGa: Experiment and density-functional theory calculations,” <i>Physical Review B - Condensed Matter and Materials Physics</i> , vol. 74, no. 5, 2006, doi: 10.1103/PhysRevB.74.054435.
[21]	Y. C. Gao and X. Gao, “The half-metallicity of LiMgPdSn-type quaternary Heusler alloys FeMnScZ (Z=Al, Ga, In): A first-principle study,” <i>AIP Advances</i> , vol. 5, no. 5, May 2015, doi: 10.1063/1.4921900.
[22]	G. D. Liu <i>et al.</i> , “Mn ₂ CoZ (Z=Al,Ga,In,Si,Ge,Sn,Sb) compounds: Structural, electronic, and magnetic properties,” <i>Physical Review B - Condensed Matter and Materials Physics</i> , vol. 77, no. 1, Jan. 2008, doi: 10.1103/PhysRevB.77.014424.
[23]	P. Klaer <i>et al.</i> , “Element-specific magnetic moments and spin-resolved density of states in CoFeMnZ (Z=Al, Ga, Si, Ge),” <i>Physical Review B - Condensed Matter and Materials Physics</i> , vol. 84, no. 14, Oct. 2011, doi: 10.1103/PhysRevB.84.144413.

[24]	Y. Jin <i>et al.</i> , “Magnetism and electronic structure of CoFeCrX (X = Si, Ge) Heusler alloys,” <i>Journal of Applied Physics</i> , vol. 120, no. 5, Aug. 2016, doi: 10.1063/1.4960350.
[25]	T. M. Bhat and D. C. Gupta, “Robust thermoelectric performance and high spin polarisation in CoMnTiAl and FeMnTiAl compounds,” <i>RSC Advances</i> , vol. 6, no. 83, pp. 80302–80309, 2016, doi: 10.1039/c6ra18934b.
[26]	S. A. Khandy and J. da Chai, “Thermoelectric properties, phonon, and mechanical stability of new half-metallic quaternary Heusler alloys: FeRhCrZ (Z = Si and Ge),” <i>Journal of Applied Physics</i> , vol. 127, no. 16, Apr. 2020, doi: 10.1063/1.5139072.
[27]	Q. Gao, H. H. Xie, L. Li, G. Lei, J. B. Deng, and X. R. Hu, “First-principle study on some new spin-gapless semiconductors: The Zr-based quaternary Heusler alloys,” <i>Superlattices and Microstructures</i> , vol. 85, pp. 536–542, Jun. 2015, doi: 10.1016/j.spmi.2015.05.049.
[28]	X. Wang, Z. Cheng, J. Wang, X. L. Wang, and G. Liu, “Recent advances in the Heusler based spin-gapless semiconductors,” <i>Journal of Materials Chemistry C</i> , vol. 4, no. 30. Royal Society of Chemistry, pp. 7176–7192, 2016. doi: 10.1039/c6tc01343k.
[29]	C. S. Lue, C. F. Chen, J. Y. Lin, Y. T. Yu, and Y. K. Kuo, “Thermoelectric properties of quaternary Heusler alloys Fe ₂ VA _{1-x} Si _x ,” <i>Physical Review B - Condensed Matter and Materials Physics</i> , vol. 75, no. 6, Feb. 2007, doi: 10.1103/PhysRevB.75.064204.
[30]	A. Kundu, S. Ghosh, R. Banerjee, S. Ghosh, and B. Sanyal, “New quaternary half-metallic ferromagnets with large Curie temperatures,” <i>Scientific Reports</i> , vol. 7, no. 1, Dec. 2017, doi: 10.1038/s41598-017-01782-5.
[31]	X. Wang <i>et al.</i> , “First-principles study of new quaternary Heusler compounds without 3d transition metal elements: ZrRhHfZ (Z = Al, Ga, In),” <i>Materials Chemistry and Physics</i> , vol. 193, pp. 99–108, Jun. 2017, doi: 10.1016/j.matchemphys.2017.02.019.

[32]	R. B. Ray, G. C. Kaphle, R. K. Rai, D. K. Yadav, R. Paudel, and D. Paudyal, "Strain induced electronic structure, and magnetic and structural properties in quaternary Heusler alloys ZrRhTiZ ($\text{Z} = \text{Al}, \text{In}$)," <i>Journal of Alloys and Compounds</i> , vol. 867, Jun. 2021, doi: 10.1016/j.jallcom.2021.158906.
[33]	Moujri, H., Berber, M., Mebrek, M. <i>et al.</i> Structural, elastic, electronic, and magnetic properties of new quaternary Heusler alloy PdCoMnGa and PdCoMnAl . <i>Indian J Phys</i> (2021).
[34]	Moujri, H., Berber, M., Mebrek, M. <i>et al.</i> Structural, elastic, electronic, and magnetic properties of new quaternary Heusler alloy PdCoMnGa and PdCoMnAl . <i>Indian J Phys</i> (2021).
[35]	S. Ahmad Khandy and J. da Chai, "Robust stability, half-metallic ferrimagnetism and thermoelectric properties of new quaternary Heusler material: A first principles approach," <i>Journal of Magnetism and Magnetic Materials</i> , vol. 502, May 2020, doi: 10.1016/j.jmmm.2020.166562.
[36]	A. Q. Seh and D. C. Gupta, "Exploration of highly correlated Co-based quaternary Heusler alloys for spintronics and thermoelectric applications," <i>International Journal of Energy Research</i> , vol. 43, no. 14, pp. 8864–8877, Nov. 2019, doi: 10.1002/er.4853.
[37]	S. Singh and D. C. Gupta, "Lanthanum based quaternary Heusler alloys LaCoCrX ($\text{X} = \text{Al}, \text{Ga}$): Hunt for half-metallicity and high thermoelectric efficiency," <i>Results in Physics</i> , vol. 13, Jun. 2019, doi: 10.1016/j.rinp.2019.102300.
[38]	B. G. Yalcin, "Ground state properties and thermoelectric behavior of Ru_2VZ ($\text{Z} = \text{Si}, \text{Ge}, \text{Sn}$) half-metallic ferromagnetic full-Heusler compounds," <i>Journal of Magnetism and Magnetic Materials</i> , vol. 408, pp. 137–146, Jun. 2016, doi: 10.1016/j.jmmm.2016.02.064.
[39]	A. Q. Seh and D. C. Gupta, "Comprehensive DFT investigation of transition-metal-based new quaternary Heusler alloys CoNbMnZ ($\text{Z} = \text{Ge}, \text{Sn}$): Compatible for spin-dependent and thermoelectric applications," <i>RSC</i>

	<i>Advances</i> , vol. 10, no. 71, pp. 43870–43881, Nov. 2020, doi: 10.1039/d0ra08007a.
[40]	S. Sharma and S. K. Pandey, “Investigation of thermoelectric properties of half-metallic Co ₂ MnGe by using first principles calculations,” <i>Journal of Physics Condensed Matter</i> , vol. 26, no. 21, May 2014, doi: 10.1088/0953-8984/26/21/215501.
[41]	A. Q. Seh and D. C. Gupta, “Comprehensive DFT investigation of transition-metal-based new quaternary Heusler alloys CoNbMnZ (Z = Ge, Sn): Compatible for spin-dependent and thermoelectric applications,” <i>RSC Advances</i> , vol. 10, no. 71, pp. 43870–43881, Nov. 2020, doi: 10.1039/d0ra08007a.
[42]	S. Sharma and S. K. Pandey, “Investigation of thermoelectric properties of half-metallic Co ₂ MnGe by using first principles calculations,” <i>Journal of Physics Condensed Matter</i> , vol. 26, no. 21, May 2014, doi: 10.1088/0953-8984/26/21/215501.



Contents lists available at ScienceDirect

Materials Today: Proceedings

journal homepage: www.elsevier.com/locate/matprInvestigation of electronic, mechanical and thermoelectric properties of quaternary Heusler compounds ZrRhTiZ ($Z = \text{In, Al}$)

Vivek Kumar, Mohit Kumar, Mukhtiyar Singh *

Department of Applied Physics Delhi Technological University, Delhi 110042, India

ARTICLE INFO

Article history:
Available online xxxxx

Keywords:
Heusler alloys
Wien2k
Half-Metallicity
Mechanical properties
Electronic properties, Thermoelectric

ABSTRACT

In the present work, a first-principles investigation of the electronic, mechanical and transport properties of quaternary Heusler compounds ZrRhTiZ ($Z = \text{In, Al}$) is reported. The observed lattice constants for ZrRhTiIn and ZrRhTiAl are 6.62 Å and 6.44 Å, respectively, which are in good agreement with earlier work. The alloys are semiconducting in spin-down state with indirect bandgap 0.39 eV and 0.30 eV for ZrRhTiIn & ZrRhTiAl , respectively but metallic in spin-up state which make them half-metallic ferromagnets. Various thermoelectric properties namely, Seebeck coefficient, electrical and thermal conductivities, and power factor are reported in the paper. The highest observed values of power factors are $1.57 \times 10^{11} \text{ W m}^{-1} \text{ K}^{-2} \text{ s}^{-1}$ and $\sim 0.66 \times 10^{11} \text{ W m}^{-1} \text{ K}^{-2} \text{ s}^{-1}$ for ZrRhTiAl and ZrRhTiIn alloys, respectively. All these properties indicate that these materials can be employed in spintronic and thermoelectric devices.

Copyright © 2022 Elsevier Ltd. All rights reserved.

Selection and peer-review under responsibility of the scientific committee of the International Conference on Materials, Processing & Characterization.

1. Introduction

Heusler alloys (HA) have recently attracted scientific attention due to their unique structural, electrical, magnetic, mechanical, and thermoelectric properties [1–3]. Among the family of Heusler alloy, Equiatomic Quaternary Heusler alloy (EQH) is one of the important categories due its application in the spintronics, magnetoelectric, magnetocaloric, ferromagnetic shape memory alloys [4–6]. EQH alloys crystallise with the Y-structure, which are more suitable for various applications than other HA because of low power dissipation. HA can be classified into three categories depending upon the stoichiometry, viz. (1) Half-Heusler (XYZ), (2) full-Heusler (X_2YZ) and (3) quaternary Heusler (XX'YZ), where X, X', and Y are transition metal elements, and Z is an element from the main group [7,8]. The EQH has space group $216-F43m$ with atoms X and X' at the 4a (0, 0, 0) and 4b (0.5, 0.5, 0.5) positions, atom Y at the 4c (0.25, 0.25, 0.25) position, and main group element Z at the 4d position (0.75, 0.75, 0.75) [9]. The occupation rule aids in the formation of a highly ordered rather than disorderly structure. Various quaternary Heusler compounds have

been described as novel Half-metals using both experimental and theoretical studies. The ZrFeTiZ ($Z = \text{Ge, Al, Si}$), ZrFeTiZ ($Z = \text{In, Al, Ga}$), and ZrCoTiZ ($Z = \text{Ga, Al, Ge, Si}$) are Zr-based EQH alloys that have been explored for spin-gapless semiconductors [10,11].

Heusler alloy has thermoelectric properties that allows it to transform heat energy into electrical energy (Seebeck effects) [12]. It's a promising attribute of HA since it can be exploited in electronic refrigeration and power generating applications that transfer heat to electricity [13,14]. Certain parameters, such as the Seebeck coefficient, electrical and thermal conductivities as a function of chemical potential and temperature, can be investigated to estimate the thermoelectric efficiency. This study uses DFT and the BoltzTraP code to report on the structural, electrical, mechanical, and thermoelectric properties of ZrRhTiZ ($Z = \text{In, Al}$).

2. Computational methodology

The Density functional theory (DFT) was used to determine various parameters of the ZrRhTiZ ($Z = \text{In, Al}$) alloys. In the work, the extremely accurate all electrons linearized augmented plane wave approach developed in the WIEN2k code was used. The Perdew–Burke–Ernzerhof generalised gradient approximation (GGA-PBE) and Tran–Blaha modified Becke–Johnson (TB-mBJ) methods were used to derive the results. When the GGA approach has been

* Corresponding author.

E-mail addresses: mukhtiyarsingh@dtu.ac.in, msphysik09@gmail.com (M. Singh).<https://doi.org/10.1016/j.matpr.2022.04.483>

2214-7853/Copyright © 2022 Elsevier Ltd. All rights reserved.

Selection and peer-review under responsibility of the scientific committee of the International Conference on Materials, Processing & Characterization.

employed, the band gap results have been underestimated. To overcome erroneous estimated values, the Tran-Blaha modified Becke-Johnson approach was used. The structural relaxation for different compositional occupancy has been achieved with RK_{max} (plane wave cutoff) is set to 7 and a converged ground state is created utilising a fine k-mesh with 8000 k-point in the Full Brillouin-zone. Finer convergence has been achieved for the energy and charge estimation at the cost of the convergence threshold 0.0001 Ry and 0.001 e, respectively. In addition, the separation of valence and core states has a cut-off energy of -6.0 Ry. Highest vector magnitude in charge density Fourier expansion (G_{\max}) = 13. The Boltzmann transport theory (BoltzTraP code) was used to determine the transport parameters of EQH ZrRhTiZ (Z = In, Al).

3. Results and discussion

3.1. Structural properties

The quaternary Heusler alloy XX'YZ are reported to have 3 possible configurations depending on how the atoms are arranged. The positions of X, X', Y, and Z atom are at 4c, 4d, 4b, and 4a; 4b, 4d, 4a and 4c; 4c, 4b, 4d and 4a, respectively [15]. The current ZrRhTiZ (Z = In, Al) is found to be most stable in Type-1. The energy minimization approach was used to find the equilibrium lattice parameter. The Birch-Murnaghan equation is explored to determine the lattice parameter and the energy for ground state at equilibrium volume. The obtained equilibrium lattice parameters are found to be 6.63 Å and 6.45 Å, respectively for ZrRhTiIn and ZrRhTiAl. Fig. 1(a) and (b) shows the volume vs energy curve of ZrRhTiIn and ZrRhTiAl respectively.

3.2. Electron density

Understanding the chemical characteristics of elements and the bonding between atoms relies heavily on electron density charts. Fig. 2 (a) and (b) shows the electron density contour plot of both the EQH's along the 110 Plane, which helps us to know the chemical bonding in the alloys. Electron density plots also help us to understand the d-d hybridization via contour plots. It can be observed that the charge accumulations between the Zr-Ti atoms is comparatively less than Rh-Ti atoms and Rh-Al/In atoms indicating in Zr-Ti interacting via ionic bond while Rh-Ti and Rh-Al/In interacting via covalent band.

3.3. Mechanical properties

$c_{11} - c_{12} > 0, c_{11} + 2c_{12} > 0, c_{44} > 0$ Within the born-stability conditions, the elastic parameters were estimated to forecast the stability of the ZrRhTiZ (Z = In, Al) alloy [16]. i.e., The estimated elastic constants are shown in Table 1. It is observed that each material satisfies the stability conditions hence are mechanically stable. The following formula is used to compute the bulk modulus B [17];

$$B = \frac{C_{11} + C_{12}}{3} \quad (1)$$

The elastic constants are used to compute the shear modulus (G), Young's modulus (E), and compressibility, which are calculated using the conventional relationships listed below [17].

$$E = \frac{9BG_H}{3B + G_H} \quad (2)$$

$$G = C_{44} \quad (3)$$

$$\beta = \frac{1}{B} \quad (4)$$

The Poisson ratio (ν) is a measurement of a material's ductility or fragility, and is represented as follows [17]:

$$\nu = \frac{1}{2} - \frac{E}{6B} \quad (5)$$

Furthermore, the Zener's value (A) can be calculated using the following equation [17]:

$$A = \frac{2C_{44}}{C_{11} - C_{12}} \quad (6)$$

It is commonly understood that if A equals one unit, the system is isotropic and anisotropic otherwise.

Reuss shear modulus, Cauchy's pressure, Voigt shear modulus, and Hill shear modulus all have the same formula [17].

$$G_p = C_{12} - C_{44} \quad (7)$$

$$G_R = \frac{5(C_{11} + C_{12})C_{44}}{4C_{44} + 3(C_{11} - C_{12})} \quad (8)$$

$$G_v = \frac{C_{11} - C_{12} + 3C_{44}}{5} \quad (9)$$

$$G_H = \frac{G_R + G_v}{2} \quad (10)$$

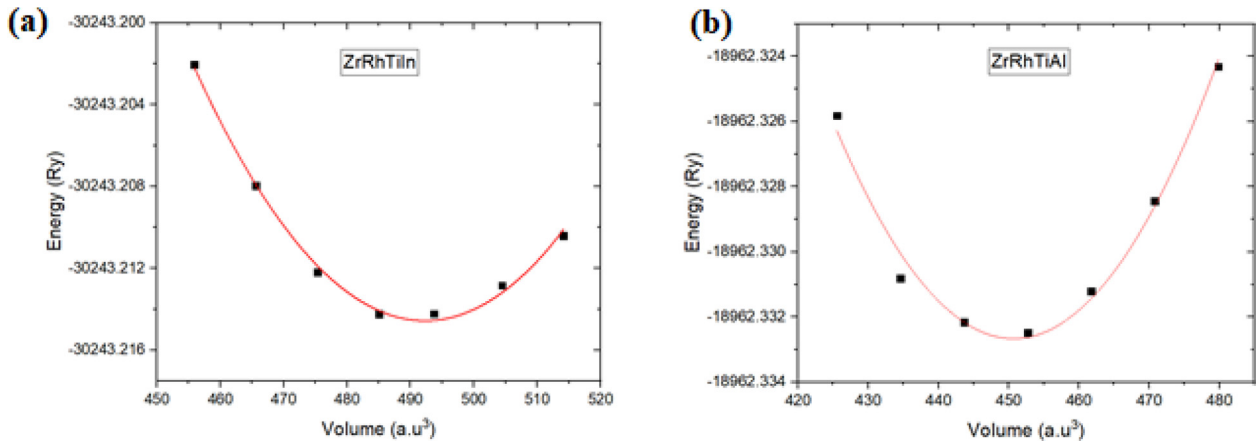


Fig. 1. (a) Energy vs Volume curve of ZrRhTiIn and (b) ZrRhTiAl.

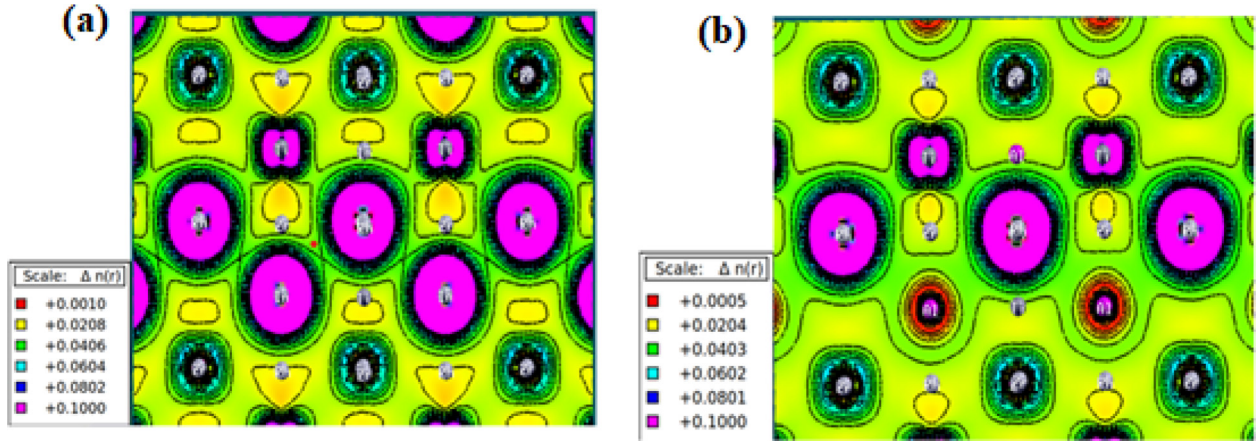


Fig. 2. Electronic charge density contour in (110) plane for (a) ZrRhTiIn and (b) ZrRhTiAl.

Table 1

Calculated elastic parameters for the ZrRhTiIn and ZrRhTiAl Heusler alloys.

Elastic parameters	ZrRhTiIn	ZrRhTiAl
C_{11} (GPa)	144.381	134.209
C_{12} (GPa)	118.126	128.502
C_{44} (GPa)	44.592	54.788
$C_{11} - C_{12}$ (GPa)	27.552	12.737
$C_{11} + 2C_{12}$ (GPa)	380.663	391.213
G (shear modulus) (GPa)	44.592	54.788
C_p (Cauchy's pressure) (GPa)	73.534	73.714
B (Bulk modulus) (GPa)	126.445	126.395
β (compressibility)	0.007908	0.007911
Pugh's ratio (B/G)	2.8355	2.306
A (Zener's value)	3.2369	8.602
G_R (Reuss shear modulus) (GPa)	23.5342	13.557
G_V (Voigt shear modulus) (GPa)	160.031	340.0142
G_H (Hill shear modulus) (GPa)	91.7826	23.7858
E (young's modulus) (GPa)	221.704	67.1454
ν (Poisson coefficient)	0.207	0.41146

$$\text{Pugh's ratio} = \frac{B}{G} \quad (11)$$

The (B/G) Pugh's ratio helps us to understand nature of the material whether it is ductile (greater than 1.75) or brittle (<1.75)[18]. The computed Pugh's ratio for ZrRhTiIn is 2.83, indicating that the material is ductile, whereas the Pugh's ratio for ZrRhTiAl is 2.30, indicating that the material is also ductile. The Cauchy pressure ($C_{12}-C_{44}$), which is positive for ductile materials and negative for brittle, supports this. Poisson ratio predicts the nature of the forces present, $\nu < 0.25$ suggest the presence of non-central force, while $0.25 \leq \nu \leq 0.50$ indicates central force. The calculated Poisson ratio for ZrRhTiIn is 0.20 which suggests the presence of non-central force while it is 0.41 for ZrRhTiAl which suggests the presence of central force. Poisson ratio can also help in understanding more about the nature of bonding. If ν is near to or more than 0.25 then it signifies the ionic bonding while it is <0.25 it signifies the covalent bonding. Zener's value (A) is found to be 3.23 for ZrRhTiIn and 8.60 for ZrRhTiAl which shows that both the materials are anisotropic (other than unity) [19].

3.4. Electronic properties

We have plotted the spin-polarized band structure using the TB-mBJ potential. Both materials, ZrRhTiZ (Z = In, Al), behave as metal for the spin up channel and exhibit semiconducting nature in the spin down channel, with a band gap at the Fermi level. The value of this band gap is 0.39 eV for ZrRhTiIn and 0.30 eV for

ZrRhTiAl. The valence band maximum and conduction band minimum are respectively situated at Γ and L, revealing a ZrRhTiZ (Z = In, Al) alloys have indirect band gap. (Figs. 3 and 4). The occurrence of a band gap at the fermi level in the down spin state implies that these alloys have 100 % spin polarization.

There are three possible explanations for the origin of the band gap in Heusler alloy. 1) - covalent bonding, 2) d-d hybridization, 3) - charge transfer. The hybridization of the Zr-4d and Rh-4d atoms forms 5 bonding bands (BB) and 5 non-bonding (NB) bands in the compounds, with 3 t_{2g} and 2 e_g in BB and 2 e_u and 3 t_u in NB. The 3d orbital of the Ti hybridised with 4d orbitals of 5 Zr-Rh BB forming the bonding and antibonding bands, while 5 NB 4d orbitals remain unhybridized. As a result, 15d orbitals are assigned to the spin-up and spin-down states, which are designated as 3 t_{2g} , 2 e_g , 2 e_u , 3 t_{1u} , 3 t_{2g} , 2 e_g , organised between higher and lower energy levels. The 1 s and 3p orbitals of Z (In, Al) are completely filled and are below the 15d hybridised orbitals. Because the triple degenerated t_{1u} states are vacant, a band gap forms between the t_{1u} (NB) and t_{2g} (BB) orbitals in the spin down state.

3.5. Transport property

The BoltzTraP code, which is based on the Semi-classical Boltzmann transport theory, was used to investigate the transport behaviour of these compounds by calculating various properties i.e., Seebeck coefficient, electrical and thermal conductivities, and power factor with temperature up to 1200 K under constant relaxation time (τ)[20]. The electrical conductivity and Seebeck coefficient are calculated using the generic Boltzmann transport equation [18,21], as shown in the formulae below;

$$\sigma_{\alpha,\beta}(\varepsilon) = \sum \tau v_{\alpha}(i,k) v_{\beta}(i,k) \frac{\delta(\varepsilon - \varepsilon_{i,k})}{\delta \varepsilon} \quad (12)$$

$$S = E_i \Delta_j T^{-1} = (\sigma) \alpha^{-1} v_{\alpha,j} \quad (13)$$

Where τ , N and ε are relaxation time, number of k-points and band energy, respectively. α and β are electrical conductivity tensor indices and $v_{\alpha}(i,k)$ is group velocity.

3.5.1. Seebeck coefficient

The material with high Seebeck coefficient is considered to be a good for thermoelectric applications[22]. Fig. 5 (a-b) shows S as a function of temperature for current alloys. The obtained Seebeck Coefficient for the ZrRhTiAl is positive for the majority of temperature ranges, as shown in Fig. 5 (a), which helps us to deduce the fact that the alloy is a P-type semiconductor. The value of Seebeck

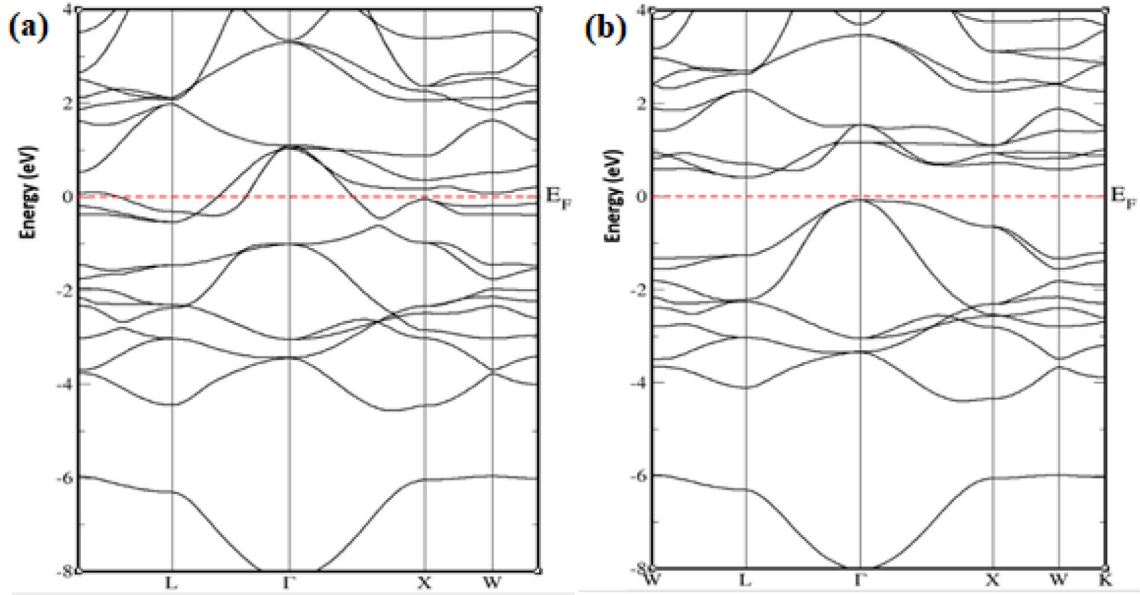


Fig. 3. Spin polarised band structure of ZrRhTiIn within the TB-mBJ approach for (a) spin up state and (b) spin down.

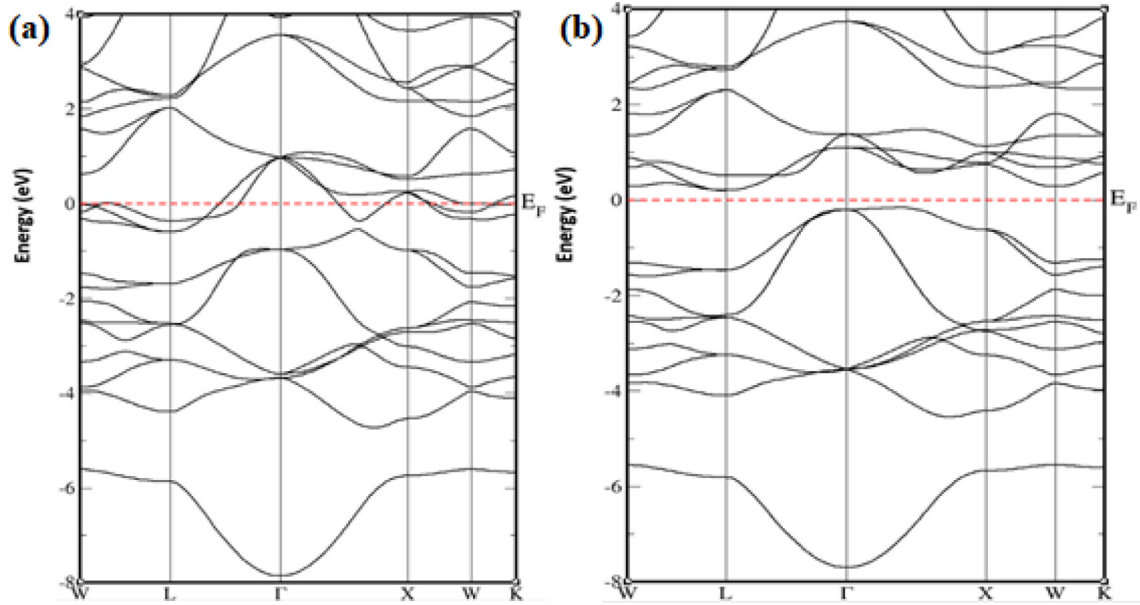


Fig. 4. Spin polarised band structure of ZrRhTiAl within the TB-mBJ approach for (a) spin up state and (b) spin down.

Coefficient starts from $\sim 15.7 \mu\text{VK}^{-1}$ at 150 K and starts falling till 550 K with value $\sim -1.83 \mu\text{VK}^{-1}$ and again increases with temperature up to $\sim 4.01 \mu\text{VK}^{-1}$ at 1200 K. At 300 K its value is $\sim 2.67 \mu\text{VK}^{-1}$ which is not so good value as compared with other materials. Fig. 5 (b) shows the variation of Seebeck coefficient for ZrRhTiIn alloys and it can be seen that for most ranges of temperature, it is negative which suggests that this alloy is a N-type semiconductor. Its value starts from $\sim -101.2 \mu\text{VK}^{-1}$ at 150 K, then decreases till $\sim -9.20 \mu\text{VK}^{-1}$ at 350 K and then again goes into positive value with an increase in temperature up to 800 K with the value of $5.47 \mu\text{VK}^{-1}$. Its value at room temperature is around $-25.40 \mu\text{VK}^{-1}$ suggesting that it is better than the former for energy conservation.

3.5.2. Electrical conductivity (σ/τ)

The amount of electric charge or heat that may pass through the Fermi level is measured by electrical conductivity. Fig. 6(a--b) depicts the fluctuation in electrical conductivity (σ) with temperature (T) for both alloys. From the Fig. 6 (a) we can see that electrical conductivity value first increases as temperature increases, from $\sim 65.6 \times 10^{20} (\Omega\text{ms})^{-1}$ at 150 K to $\sim 73.0 \times 10^{20} (\Omega\text{ms})^{-1}$ at 600 K and starts decreases till $\sim 71.7 \times 10^{20} (\Omega\text{ms})^{-1}$ at 1200 K, the value of the electrical conductivity at room temperature is $\sim 71.23 \times 10^{20} (\Omega\text{ms})^{-1}$ for ZrRhTiAl alloy. The electrical conductivity of the ZrRhTiIn alloy shows a roughly linear fluctuation with temperature, as shown in Fig. 6 (b). The value of electrical conductivity starts from $\sim 0.049 \times 10^{20} (\Omega\text{ms})^{-1}$ at 150 K increases

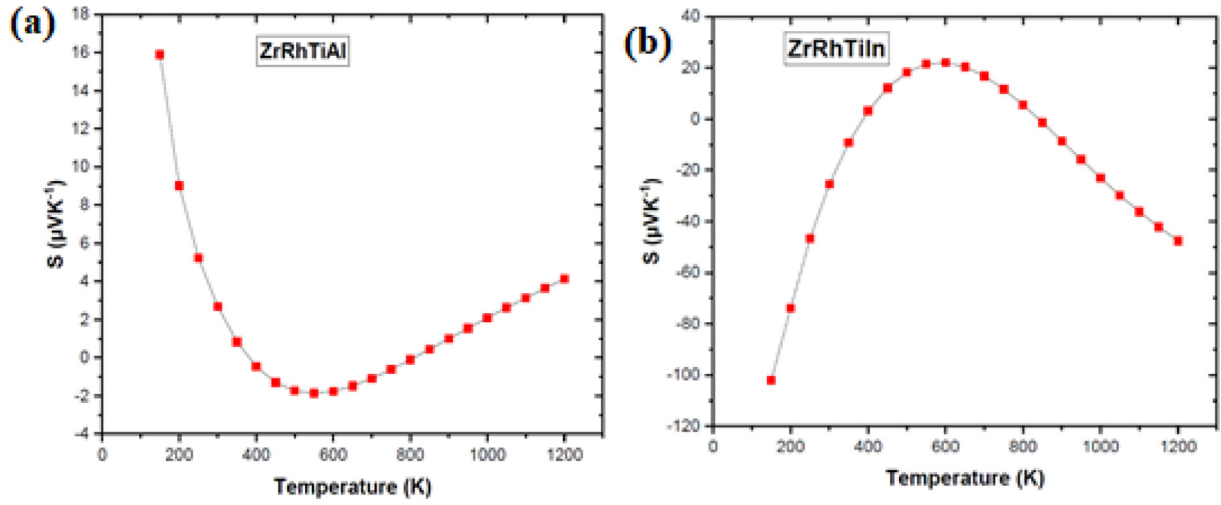


Fig. 5. Seebeck coefficient variation with temperature for (a) ZrRhTiAl and (b) ZrRhTiIn.

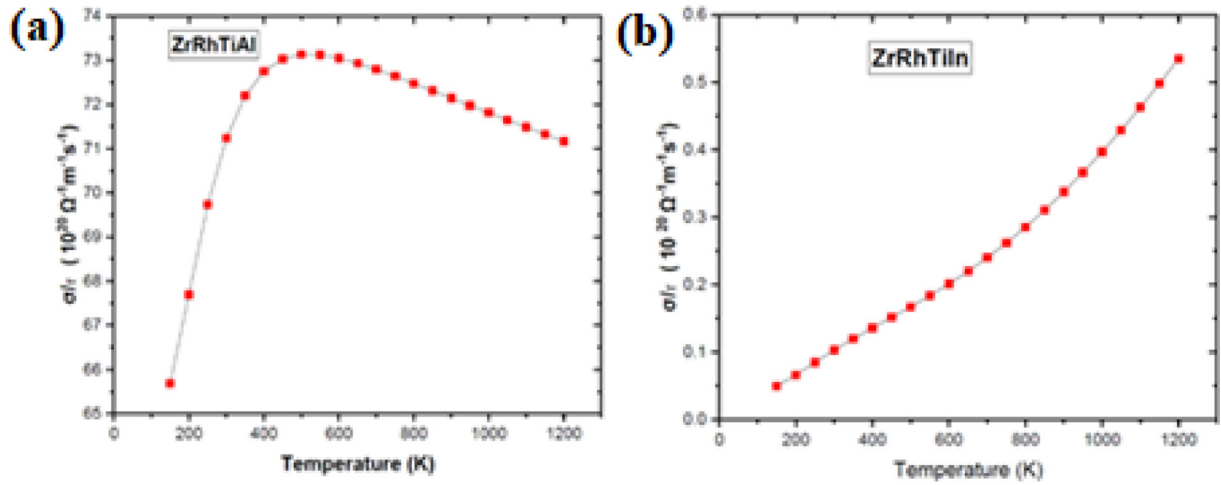


Fig. 6. electrical conductivity variation with temperature for (a) ZrRhTiAl and (b) ZrRhTiIn.

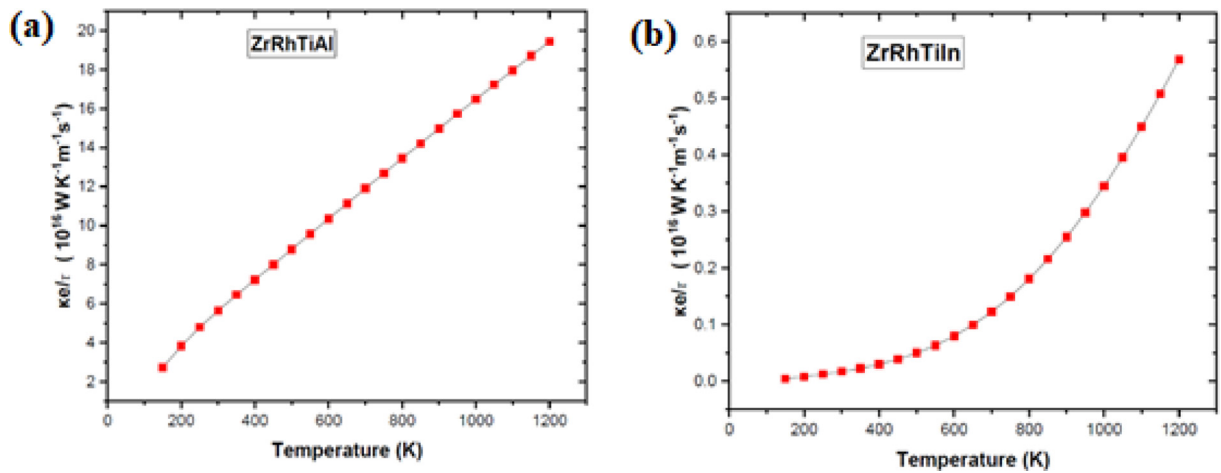


Fig. 7. Variation of electronic thermal conductivity with temperature for (a) ZrRhTiAl and (b) ZrRhTiIn.

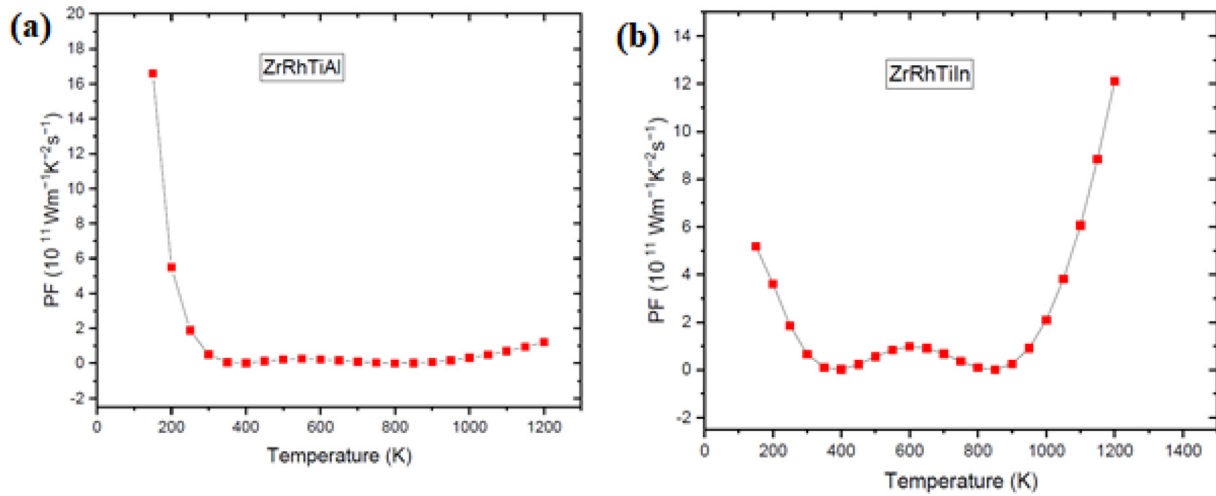


Fig. 8. Power factor variation with temperature for (a) ZrRhTiAl and (b) ZrRhTiIn.

as the temperature rises. The value of σ/τ at 1200 K is $0.535 \times 10^{20} \cdot (\Omega\text{ms})^{-1}$ and the value of electrical conductivity for room temperature is $\sim 0.103 \times 10^{20} (\Omega\text{ms})^{-1}$.

3.5.3. Electronic thermal conductivity (κ_e/τ)

A material's thermoelectric performance is inversely proportional to its thermal conductivity. Therefore, for better thermoelectric efficiency, it should be very low [23]. Fig. 7(a–b) shows the variation in the electrical part of thermal conductivity with varying of temperature. Fig. 7(a) depicting that, that the electronic thermal conductivity increases linearly from $\sim 2.72 \times 10^{16} (\text{W m}^{-1}\text{K}^{-1}\text{s}^{-1})$ to $19.4 \times 10^{16} (\text{W m}^{-1}\text{K}^{-1}\text{s}^{-1})$ for the ZrRhTiAl. The value of electronic thermal conductivity at room temperature is $\sim 5.64 \times 10^{16} (\text{W m}^{-1}\text{K}^{-1}\text{s}^{-1})$. Similarly, Fig. 7(b) shows that it increases exponentially as temperature rises from $0.043 \times 10^{16} (\text{W m}^{-1}\text{K}^{-1}\text{s}^{-1})$ to $0.568 \times 10^{16} (\text{W m}^{-1}\text{K}^{-1}\text{s}^{-1})$ with room temperature value $\sim 0.017 \times 10^{16} (\text{W m}^{-1}\text{K}^{-1}\text{s}^{-1})$ for ZrRhTiIn. The ZrRhTiIn has lower value than ZrRhTiAl means that the former will be more useful as heat dissipation will be less in the ZrRhTiIn alloy.

3.5.4. Power factor

The power factor (PF) is a parameter which defines the material's efficiency for their thermoelectric application. The PF can be written as,

$$\text{PF} = S^2 \sigma / \tau \quad (15)$$

σ/τ is the electrical conductivity, and S is the Seebeck coefficient [24]. Fig. 8 (a–b) plots the PF against the temperature for both the EQH's. Fig. 8 (a) shows the plot of PF against temperature from 150 K to 1200 K for ZrRhTiAl, it can be observed that the PF has maximum value of $\sim 17.74 \times 10^{11} \text{ Wm}^{-1}\text{K}^{-2}\text{s}^{-1}$ at 150 K, as temperature increases the PF decreases till 500 K having value $\sim 0.2 \times 10^{11} \text{ Wm}^{-1}\text{K}^{-2}\text{s}^{-1}$ and again increase slowly or become nearly constant. The value of PF at room temperature is observed to be $\sim 1.57 \times 10^{11} \text{ Wm}^{-1}\text{K}^{-2}\text{s}^{-1}$ for ZrRhTiAl alloy. Similarly, the fluctuation of PF as a function of temperature for the ZrRhTiIn alloy is shown in Fig. 8 (b). It can be seen clearly that the PF has a value of $5.56 \times 10^{11} \text{ Wm}^{-1}\text{K}^{-2}\text{s}^{-1}$ at 150 K and the PF value at 1200 K is $\sim 12.11 \times 10^{11} \text{ Wm}^{-1}\text{K}^{-2}\text{s}^{-1}$. The value of PF at room temperature is observed to be $\sim 0.66 \times 10^{11} \text{ Wm}^{-1}\text{K}^{-2}\text{s}^{-1}$.

4. Conclusions

In this present paper, we examined the equiatomic quaternary Heusler alloys ZrRhTiIn and ZrRhTiAl using the density functional theory approach and semi-classical methods for its electronic, mechanical and thermoelectric properties. Both the alloys have found to be semiconducting in spin-down state with an indirect band gap. Because of the small band gap, they are useful for thermoelectric applications. The observed results for band gap agree with the previously reported results [25]. The Seebeck coefficient for ZrRhTiIn is $-25.40 \mu\text{VK}^{-1}$ and for ZrRhTiAl is $\sim 2.67 \mu\text{VK}^{-1}$ at 300 K, the corresponding Power factors are $\sim 0.66 \times 10^{11} \text{ Wm}^{-1}\text{K}^{-2}\text{s}^{-1}$ and $\sim 1.57 \times 10^{11} \text{ Wm}^{-1}\text{K}^{-2}\text{s}^{-1}$, respectively. Comparatively, ZrRhTiIn is a more promising thermoelectric material than the ZrRhTiAl. The obtained values are not very well adequate for application but can be improved with appropriate electron and hole doping.

CRediT authorship contribution statement

Vivek Kumar: Conceptualization, Investigation, Writing – original draft. **Mohit Kumar:** Investigation, Data curation, Validation. **Mukhtiyar Singh:** Supervision, Methodology, Writing – review & editing.

Declaration of Competing Interest

The authors declare that they have no known competing financial interests or personal relationships that could have appeared to influence the work reported in this paper.

Acknowledgment

The authors wish thanks the University Grants Commission (UGC) of India for funding the computational facilities at the Department of Applied Physics, Delhi Technological University, Delhi, India, under the START-UP GRANT (No. F.30-416/2018 (BSR), dated 18/09/2018).

References

- [1] X. Wang, Z. Cheng, J. Wang, X.-L. Wang, G. Liu, Recent advances in the Heusler based spin-gapless semiconductors Liu, J. Mater. Chem. C 4 (30) (2016) 7176–7192.
- [2] T.M. Bhat, D.C. Gupta, Robust thermoelectric performance and high spin polarisation in CoMnTiAl and FeMnTiAl compounds, RSC Adv. 6 (83) (2016) 80302–80309.
- [3] Lue C. S, C. F. Chen, J. Y. Lin, Y. T. Yu, and Y. K. Kuo, Thermoelectric properties of quaternary Heusler alloys Fe₂VA1_{1-x}Si_x. *Phys. Rev. B* 2007;75:064204.
- [4] L. Bainsla, K.G. Suresh, Equiatomic quaternary Heusler alloys: A material perspective for spintronic Applications, *Appl. Phys. Rev.* 3 (3) (2016) 031101.
- [5] A. Kundu, S. Ghosh, R. Banerjee, S. Ghosh, B. Sanyal, New quaternary half-metallic ferromagnets with large Curie temperatures, *Sci. Rep.* 7 (1) (2017).
- [6] H. Alqurashi, B. Hamad, Magnetic structure, mechanical stability and thermoelectric properties of VTiRhZ (Z = Si, Ge, Sn) quaternary Heusler alloys: first-principles calculations, *Appl. Phys. A* 127 (10) (2021).
- [7] M. Singh, H.S. Saini, S. Kumar, M.K. Kashyap, Effect of substituting sp-element on half metallic ferromagnetism in NiCrSi Heusler alloy, *Comput. Mater. Sci.* 53 (1) (2012) 431–435.
- [8] M. Singh, H.S. Saini, J. Thakur, A.H. Reshak, M.K. Kashyap, Electronic structure, magnetism and robust half-metallicity of new quaternary Heusler alloy FeCrMnSb, *J. Alloys. Compd.* 53 (2013) 201–204.
- [9] I. Galanakis, P.H. Dederichs, N. Papanikolaou, Slater-Pauling behavior and origin of the half-metallicity of the full-Heusler alloys, *Phys. Rev. B* 66 (17) (2002).
- [10] Q. Gao, H.H. Xie, L. Li, G. Lei, J.B. Deng, X.R. Hu, First-principle study on some new spin-gapless semiconductors: The Zr-based quaternary Heusler alloys, *Superlattices Microstruct.* 85 (2015) 536–542.
- [11] S. Yousuf, D.C. Gupta, Investigation of electronic, magnetic and thermoelectric properties of Zr₂Ni (Z = Al, Ga) ferromagnets, *Mater. Chem. Phys.* 192 (2017) 33–40.
- [12] A.A. Mubarak, S. Saad, F. Hamioud, M. Al-Elaimi, Structural, thermo-elastic, electro-magnetic and thermoelectric attributes of quaternary CoNbMnX (X = Al, Si) Heusler alloys, *Solid State Sci.* 111 (2021) 106397.
- [13] S.A. Sofi, D.C. Gupta, Systematic study of ferromagnetic phase stability of Co-based Heusler materials with high figure of merit: Hunt for spintronics and thermoelectric applicability, *AIP Adv.* 10 (10) (2020) 105330.
- [14] S. Sharma, S.K. Pandey, Investigation of thermoelectric properties of half-metallic Co₂MnGe by using, first principles calculations, *J. Phys. Condens. Matter.* 26 (21) (2014) 215501.
- [15] S. Ghosh, S. Ghosh, Half-Metallicity in Quaternary Heusler Alloys with 3d and 4d Elements: Observations and Insights from DFT Calculations, *Phys. Status Solidi B* 256 (8) (2019) 1900039.
- [16] S. Berri, Computational Study of Structural, Electronic, Elastic, Half-Metallic and Thermoelectric Properties of CoCrScZ (Z=Al, Si, Ge, and Ga) Quaternary Heusler Alloys, *J. supercond. Nov. Magn.* 33 (12) (2020) 3809–3818.
- [17] H. Moujri, M. Berber, M. Mebrek, A. Boudali, T. Ouahrani, Structural, elastic, electronic, and magnetic properties of new quaternary Heusler alloy PdCoMnGa and PdCoMnAl. *Indian, J. Phys.* 96 (4) (2022) 1025–1035.
- [18] S. Ahmad Khandy, J.-D. Chai, Robust stability, half-metallic ferrimagnetism and thermoelectric properties of new quaternary Heusler material: A first principles approach, *J. Magn. Magn.* 502 (2020) 166562.
- [19] Khandy S. A and J. da Chai, Thermoelectric properties, phonon, and mechanical stability of new half-metallic quaternary Heusler alloys: FeRhCrZ (Z = Si and Ge). *J. Appl. Phys.* 2020;127:165102.
- [20] A.Q. Seh, D.C. Gupta, Comprehensive DFT investigation of transition-metal-based new quaternary Heusler alloys CoNbMnZ (Z = Ge, Sn): Compatible for spin-dependent and thermoelectric applications, *RSC Adv.* 10 (71) (2020) 43870–43881.
- [21] Khandy S. A. I. Islam, D.C Gupta, M. A. Bhat, S. Ahmed, T. A. Dar, S. Rubab, S. Dhiman and A. Laref, A case study of Fe₂TaZ (Z = Al, Ga, In) Heusler alloys: hunt for half-metallic behaviour and thermoelectricity. *RSC Adv.* 2018;8:40996–41002.
- [22] A.Q. Seh, D.C. Gupta, Exploration of highly correlated Co-based quaternary Heusler alloys for spintronics and thermoelectric applications, *Int. J. Energy Res.* 43 (2019) 8864–8877.
- [23] S. Singh, D.C. Gupta, Lanthanum based quaternary Heusler alloys LaCoCrX (X = Al, Ga): Hunt for half-metallicity and high thermoelectric efficiency, *Results in Phys.* 13 (2019) 102300.
- [24] T.T. Lin, Q. Gao, G.D. Liu, X.F. Dai, X.M. Zhang, H.B. Zhang, Dynamical stability, electronic and thermoelectric properties of quaternary ZnFeTiSi Heusler compound, *Curr. Appl. Phys.* 19 (6) (2019) 721–727.
- [25] R.B. Ray, G.C. Kaphle, R.K. Rai, D.K. Yadav, R. Paudel, D. Paudyal, Strain induced electronic structure, and magnetic and structural properties in quaternary Heusler alloys ZrRhTiZ (Z = Al In), *J. Alloys compd.* 867 (2021) 158906.



Source details

Materials Today: Proceedings

Scopus coverage years: 2005, from 2014 to Present

E-ISSN: 2214-7853

Subject area: [Materials Science: General Materials Science](#)

Source type: Conference Proceeding

[View all documents >](#)[Set document alert](#) [Save to source list](#) [Source Homepage](#)

CiteScore 2020

1.8



SJR 2020

0.341



SNIP 2020

0.657



[CiteScore](#) [CiteScore rank & trend](#) [Scopus content coverage](#)

i Improved CiteScore methodology



CiteScore 2020 counts the citations received in 2017-2020 to articles, reviews, conference papers, book chapters and data papers published in 2017-2020, and divides this by the number of publications published in 2017-2020. [Learn more >](#)

CiteScore 2020

$$1.8 = \frac{27,773 \text{ Citations 2017 - 2020}}{15,346 \text{ Documents 2017 - 2020}}$$

Calculated on 05 May, 2021

CiteScoreTracker 2021

$$2.3 = \frac{48,786 \text{ Citations to date}}{21,371 \text{ Documents to date}}$$

Last updated on 06 April, 2022 • Updated monthly

CiteScore rank 2020

Category	Rank	Percentile
Materials Science		
General Materials Science	#280/455	38th

[View CiteScore methodology >](#) [CiteScore FAQ >](#) [Add CiteScore to your site](#)

About Scopus

[What is Scopus](#)

[Content coverage](#)

[Scopus blog](#)

[Scopus API](#)

[Privacy matters](#)

Language

[日本語に切り替える](#)

[切换到简体中文](#)

[切换到繁體中文](#)

[Русский язык](#)

Customer Service

[Help](#)

[Tutorials](#)

[Contact us](#)

ELSEVIER

[Terms and conditions ↗](#) [Privacy policy ↗](#)

Copyright © Elsevier B.V. ↗. All rights reserved. Scopus® is a registered trademark of Elsevier B.V.

We use cookies to help provide and enhance our service and tailor content. By continuing, you agree to the use of cookies.

